Peptide Directed 3D Assembly of Nanoparticles through Biomolecular Interaction

by

Prerna Kaur

A Dissertation submitted to Graduate Faculty in Biochemistry in partial
fulfillment of the requirements for the degree of Doctor of Philosophy,
The City University of New York

2012

This manuscript has been read and accepted for the Graduate Faculty in Biochemistry in satisfaction of the dissertation requirement for the degree of Doctor of Philosophy

Prof. Hiroshi Matsui, Hunter College

Date
Chair of Examining Committee

Prof. Edward Kennelly

Date
Executive Officer

Prof. Charles M. Drain, Hunter College

Prof. Alexander Couzis,City College

Prof. Ronald Koder, City College

Prof. Yujia Xu,Hunter College

Supervisory Committee

THE CITY UNIVESITY OF NEW YORK

ABSTRACT

Peptide Directed 3D Assembly of Nanoparticles through Biomolecular Interaction

by

Prerna Kaur

Advisor: Professor Hiroshi Matsui

The current challenge of the ‘bottom up’ process is the programmed self-assembly of nanoscale building blocks into complex and larger-scale superstructures with unique properties that can be integrated as components in solar cells, microelectronics, metamaterials, catalysis, and sensors. Recent trends in the complexity of device design demand the fabrication of three-dimensional (3D) superstructures from multi-nanomaterial components in precise configurations. Biomimetic assembly is an emerging technique for building hybrid materials because living organisms are efficient, inexpensive, and environmentally benign material generators, allowing low temperature fabrication.

Using this approach, a novel peptide-directed nanomaterial assembly technology based on biomolecular interaction of streptavidin and biotin is presented for assembling nanomaterials with peptides for the construction of 3D peptide–inorganic superlattices with defined 3D shape. We took advantage of robust natural collagen triple-helix peptides and used them as nanowire building blocks for 3D peptide– gold nanoparticles superlattice generation.

The type of 3D peptide superlattice assembly with hybrid NP building blocks described herein shows potential for the fabrication of complex functional device which demands precise long-range arrangement and periodicity of NPs.

ACKNOWLEDGMENTS

I would like to express my sincere gratitude to my advisor, Prof. Hiroshi Matsui, for his constant encouragement and guidance. His innovative ideas and zeal for cutting edge research lead me to the world of bio-nanotechnology and made it possible to finish this thesis.

I am also extremely thankful to my committee members, Prof. Micheal C.Drain, Prof. Alexander Couzis, Prof. Ronald L.Koder and Prof. Yujia Xu, for their constructive comments and constant support throughout this work. I thank my past and present group members in Matsui's group for their friendship and wonderful collaboration throughout my PhD years. I would like to thank the Department of Chemistry at Hunter College and the Graduate Center of City University of New York.

Most importantly, I am thankful to my Parents, Brother and Husband whose love and support made this possible.

Special thanks to my husband, Harpreet, for his endless support and encouragement throughout my research life and in writing my thesis. It was impossible to complete this thesis in time without his help.

Table of Contents

List of Tables

List of Figures

CHAPTER 1: PROTEIN AS A BIOMIMETIC TEMPLATE FOR THE ASSEMBLY OF NANOPARTICLES

1.1 Introduction

The current challenge of the bottom up approach is the programmed control of self-assembly of nanoscale components to achieve three-dimensional supramolecular architectures with defined functionalities. We have reached the theoretical lower limit of nanofabrication miniaturization, as top down approach of ion and electron-beam lithography get increasingly time consuming and expensive at scales below 100nm. Therefore, to control the 3D precision, one particular potential approach involves the use of hybrid system, in which existing lithographic techniques are associated with 'bottom up' approach such as supramolecular self-assembly. Biomolecular systems combine both self-organization and spatial ordered patterning at the nanometer length scale providing a new nanofabrication protocol.

This emerging field of nano biotechnology explicitly uses the tool box of biological entities with nanomaterials in controlling, and applying biomolecule-nanomaterial interactions for designing devices and hybrid materials which then can be fabricated and characterized for magnetic, optical, electronic, and sensor applications by retaining the structural and functional activity of the biomolecule. Moreover, the distance and strength of the interaction can be tuned using biomolecule-directed strategies. Low production costs; and the ability to be optimized for large scale production by decorating the surface of biomolecule makes this class of material a useful candidate for ‘bottom up’ strategy.

1.2 Biomolecule Directed Nanoparticle Assembly

Initial work has shown that complementary strands of DNA molecules were used to self-assemble inorganic nanoparticles. One of earlier work of constructing 3D architecture was carried out using DNA by Seemam[1] who reported 3D DNA objects with the topology of a cube and a truncated octahedron and Mirkin[2] and Gang[3] created 3D gold nanoparticle crystals with long-range order by modifying gold nanoparticles with single-stranded DNA, which allowed them to control crystallization and spacing of nanoparticle. But, the questions arises: Can DNA be used as a material that is robust enough to resist extreme temperatures and stimuli responsive which can be tailored for long term high throughput electronic(ultra small circuits) and chip design applications?

Proteins have emerged as a major building block for the development of new class of bio- materials. The ability to self-assemble due to their unique properties such as recognition (molecular epitopes) functional components, monodispersity, and biofabrication is specific to each family of protein. The techniques of genetic engineering enable the design and synthesis, resulting in mass production of proteins. Also, the formation of peptide based nanostructures[4] through the process of 'self assembly' mediated by weak noncovalent interactions has led to the formation of new class of self assembled nanostructures [5, 6] for regenerative medicine.

1.3 Protein Mediated Nanoparticle Assembly

The ability to synthesize protein based hybrid functional material combines the features of tunable nanopaticles with the biological functionality of the protein. The strength and selectivity of protein-protein interactions make proteins an excellent template to serve as scaffold, linkers and template between nanoparticles to form ordered super structures. For example an antigen-antibody interaction[7-9] was used by Kotov and collaborators to assemble junctions of pre-assembled wires of semiconducting CdTe. [10] Mann[7] and coworkers used antigen-antibody recognition to directly assemble nanoparticles into micron size materials and also applied biotin-streptavidin interactions for programmed aggregation of iron oxide nanoparticles in biotinylated ferritin by streptavidin connectors. Bacterial S-layer proteins have been used for the deposition and growth of nanoparticles into two-dimensional crystals on flat substrates.[11-12] Proteins preassembled into microtubules [13-14] have been used to direct the assembly of nanoparticles. Biotin-streptavidin interactions[15-17] were employed by Searson's[18] group to direct the end-to-end assembly of Au/Pt/Au nanowires. Caswell et al.observed that biotin-functionalized gold nanorods can be preferentially assembled in an end-to-end fashion using a streptavidin linker. Smorodin and colleagues assembled carbon nanotubes and gold nanoparticles using biotin and streptavidin. Belcher and coworkers used genetically modified M13 viruses to display streptavidin-binding peptide and hexahistidine peptide[19] at opposite ends and demonstrated the assembly of the viruses into nanorings by adding a streptavidin-NiNTA. Yoo[20] and coworkers showed that the protein coat of the M13 virus could be tuned to modify the surface charge of the virus and hence its assembly on polyelectrolyte multilayers. These are some of the few examples featuring 1D and 2D assembly[21] of bionanomaterial with proteins.

The above mentioned examples apply superficial technique to assemble nanoparticles with biomolecules using ‘bottom up’ approach. Highly controlled long range ordering is required to design architectures with defined optical and electronic properties in the nanocomposites. To develop such superstructures with 3D assembly, we need proteins which are robust enough to sustain its conformation in the presence of nanomaterial with reconfiguration of its assembly based on external stimuli like pH, salt and temperature to control the spacing between the nanoparticles by incorporating its native functionality in the composites. Importantly, these external stimuli will also affect the dielectric environment of the medium by precisely adjusting the magnitude of attractive and repulsive interactions which favor the formation of critical crystal nucleus[22] by lowering the barrier of free energy which thereby triggers the crystal formation.

1.4 Applications of Biomolecules-Nanoparticle Assembly

Nanoparticle-biomolecule interactions have been applied for constructing novel devices[23 - 27] because the resulting hybrid material possess the unique optical, electrical properties of the nanoparticles combined with distinct intrinsic structural and functional characteristic features of the biomolecule. Nucleic acids and proteins were tailored to be fabricated on the nanoparticle surface for biological, diagnostic [28-34] and sensor applications.[35-37]

CHAPTER 2: THREE-DIMENSIONAL DIRECTED SELF-ASSEMBLY OF PEPTIDE NANOWIRES INTO MICROMETER-SIZED CRYSTALLINE CUBES WITH NANOPARTICLE JOINTS

2.1 Introduction

2.1.1 Biomimetic Systems

In the last decade, nanoscale materials have been created with superior physical properties. The next challenge is to assemble nanoscale building blocks into complex and larger-scale superstructures so that these nanomaterials with unique properties can be integrated as macroscale components in solar cells, microelectronics, met materials, catalysis, and sensors.[38] Recent trends in the complexity of device design demand the fabrication of three-dimensional (3D) superstructures from multi-nanomaterial components in precise configurations.[39]

Biomimetic assembly is an emerging technique in such pursuits, because living organisms are efficient, inexpensive, and environmentally benign material generators, allowing low temperature fabrication.[40-44]

Although DNA bio nanotechnology has recently been used to precisely assemble 3D shapes,[45-53] the methods to develop highly ordered macroscopic materials from these nanostructures remains limited, [54] and for practical applications the production scale, size, and the yield of the assembled materials need to be amplified.[55-56]

2.1.2 Importance of Peptide as Biomimetic Scaffold

Peptides are another of nature's building blocks with high specificity, versatility, and robustness for directed assembly that can be exploited to design novel 3D superstructures.[57] They serve as linkers, templates and scaffolds via chemical and biomolecular interactions with tunable features of nanoparticle's size, surface properties to create novel hybrid materials. By means of genetic engineering, tailor made peptides and proteins of varied length and functionality can be assembled in a cost effective manner in required quantities.

In this approach, we took advantage of the naturally robust assembling nature of collagen triple-helix peptides and used them as nanowire building blocks for 3D peptide–nanoparticle super lattice generation. This method uses the inherent properties of the peptides such as directed self assembly and stability to control the spacing of the ligand-functionalized gold nanoparticle (Au NP) joints for the development of the micrometer-scale 3D cube-shaped hybrid superlattices, creating a physical framework for the proposed biomimetic assembly strategy.

These collagen-mimicking peptides can self associate laterally, [58-59] and this intrinsic peptide–peptide interaction allows us to create unit cells of various scales and also predicts the ability to create an extensive latticework of cubic microcrystals. The NPs can join the peptide nanowires through the streptavidin–

biotin interaction to create cubic unit cells with extremely high yield and the resulting peptide–NP superlattices are ordered in the long range with the isotropic crystalline orientation. This simple and rapid fabrication method produces high yields of 3D materials in tailored shapes that are dependent on the geometry of the peptide–NP unit cells, thus promising ease and flexibility in manufacturing functional devices. To our knowledge, this is the first example of 3D NP superlattice assembly on a micrometer scale from peptide nanowires.

2.1.3 Collagen

Collagens are the most abundant family of structural proteins in the human body, and are an important constituent of ligaments, cartilage, tendons and bone. The first X-ray structure of the triple helix was reported using short synthetic peptides. This unique structure of the triple helix is made of three super coiled polyproline II-like chains. Each amino acid chain requires a Glycine at every third residue to form a unique $(\text{Gly-X-Y})_n$ repeating sequence pattern, where X and Y can be any amino acids Figure 2-1.

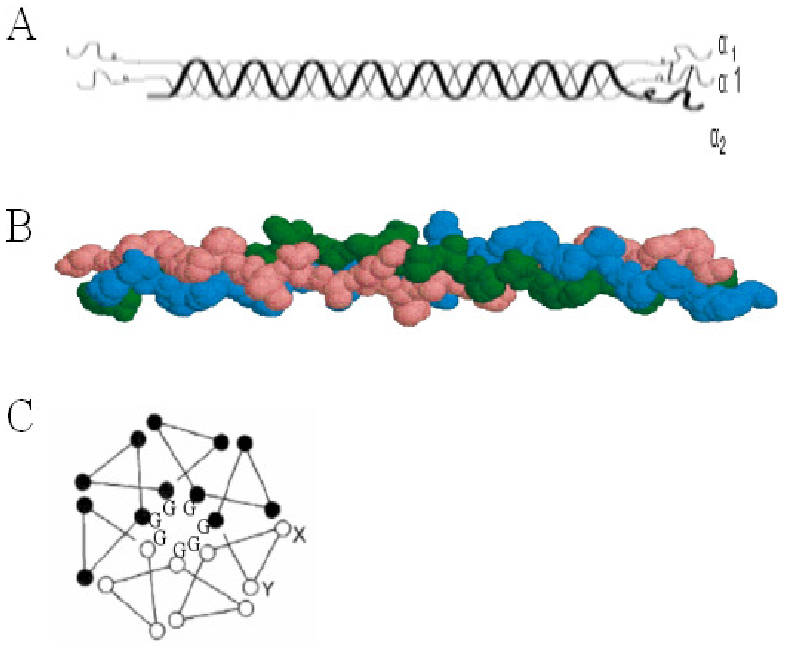

Figure 2-1: a) A representation of the triple helical structure of type I collagen heterotrimer; b) 3D triple helix structure of type I collagen; c) Top view of a type I collagen triple helix.

Glycine, the smallest amino acid in every three residues, is essential for the triple helix structure's stability because it is the only amino acid packed into the restricted space in the center of triple helix, while the other residues on X and Y positions are largely exposed to solvent. It is the frequent occurrence of proline and hydroxyproline groups in the polypeptide chain that causes the collagen a-chains to be tightly packed into a triple helical conformation. In type I collagen, the triple helix molecule is a heterotrimer comprising of two identical α1 chains and one α2 chain (Figure 2-1). The α1 and α2 chains are very similar with over 95% identity on amino acid sequence. Each α-chain contains over 1000 amino acids and has a molecular weight of approximately 95,000. These molecules of type I collagen have a length of slightly less than 300nm and diameter of about 1.4nm.

Collagens form triple helices, which provide critical building blocks for higher ordered aggregates.[60] In addition to the biomedical studies, the recombinant collagen fragments have also proven to be a good system to produce nano-templates. The rigidity of the helix backbone, the linear conformation, and the largely exposed side chains of residues at the X and Y positions for chemical modification make the triple helix an ideal template for nano wires. Genetic engineering provides a tool for the design and synthesis of polypeptides having predetermined and precisely controlled molecular architectures. Specifically, the primary amino acid sequence of a polypeptide, and the size of the polymer, may be controlled by varying the sequence and length of the encoding DNA. This strategy has been employed in the de novo design and synthesis of macromolecular materials that exhibit well-defined higher order structures. [61-62]

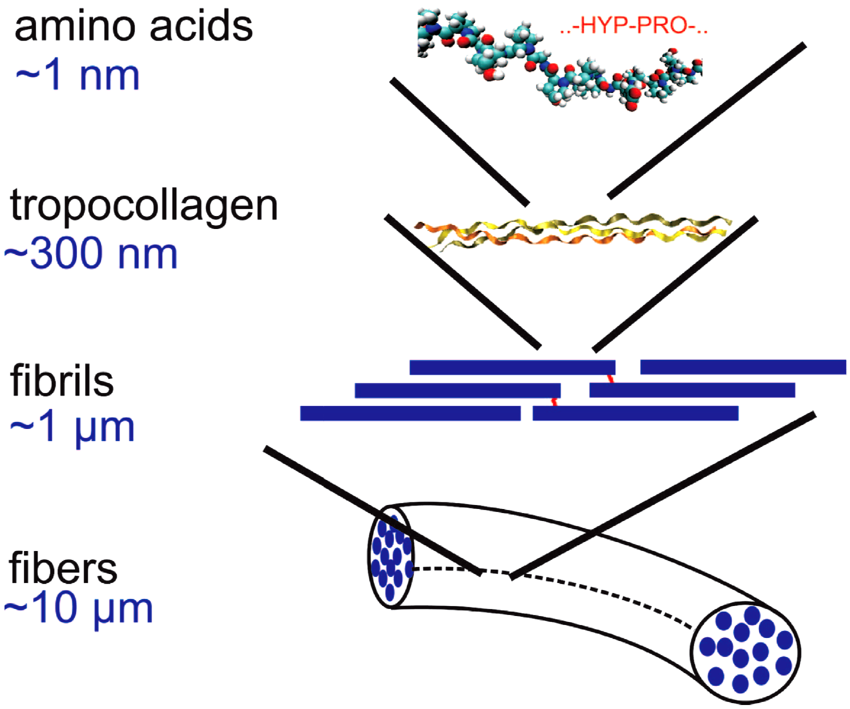

Figure 2-2: Hierarchical structural organization of collagen with amino acid sequence at nano scale up to the scale of collagen fibers in microns.[63]

Theoretical and molecular modeling suggests that this natural design of collagen fibrils maximizes the strength and provides large energy dissipation during deformation, thus creating a tough and robust material.[63]

2.2 Generation of Recombinant Collagen Protein

2.2.1 Biotin Acceptor Peptide 877(BAP 877)

The collagen peptide is derived from the F877 peptide that was previously used as a nanowire template.[64-65] This new BAP877 peptide is modified by the insertion of a 15amino acid residue of biotin acceptor peptide (BAP) [66-68] at the N terminus (Figure 2-3). Other design features of this collagen peptide include a triple-helix domain consisting of 63 residues from the a1 chain of type I collagen with additional repeating Gly-Pro-Pro sequences for increased stability, a bacteriophage T4 fibritin foldon domain at the C terminus serving as a nucleation site to facilitate the correct folding, and a Cys-knot sequence (Gly-Pro-Cys-Cys) to cross-link three polypeptide chains of the triple helix through a set of disulfide bonds (Figure 2-3).

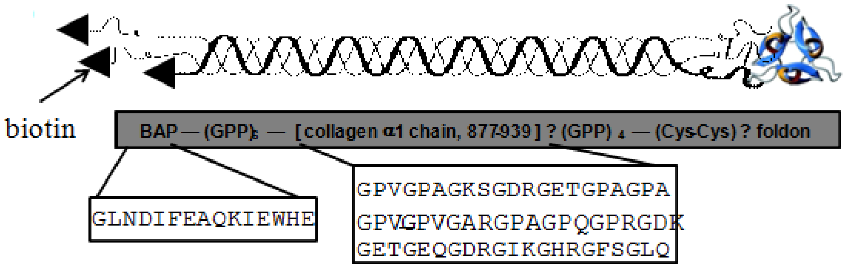

Figure 2-3: Structure of the engineered triple-helix peptide with biotin at the N terminus.

This BAP site is designed to be biotinylated in vivo to generate the complementary binding motif for streptavidin-coated Au NPs. To accomplish this modification, BAP877 peptide was expressed as a fusion protein in E. coli, where endogenous bacterial biotin ligase BirA biotinylates the specific lysine residue within the BAP sequence.[69-70] The purified biotinylated triple-helix peptide (Figure 2-4) was monodisperse in size (4× 40 nm^2) and adapted to rigid conformation with no sign of bending.

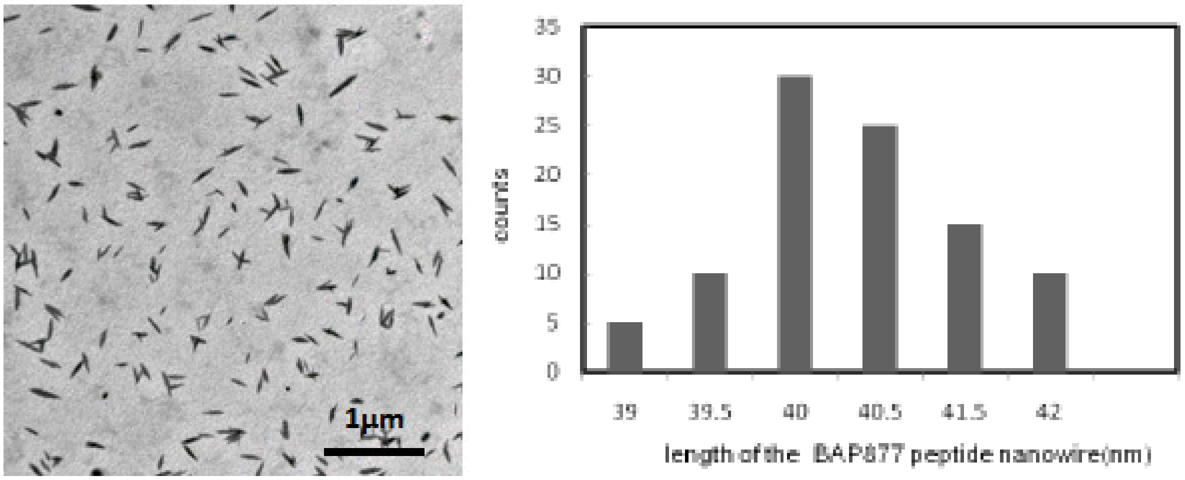

Figure 2-4: TEM image of biotinylated triple-helix peptides. Scale bar: 1μm. The length distribution of BAP877 peptides obtained from TEM images of 95 samples.

2.3 3D Assembly of Biotin Acceptor Peptide BAP877 with Streptavidin Functionalized Gold Nanoparticles

In the proposed 3D peptide–NP super lattice assembly (Figure 2-5); the biotin–streptavidin interaction joins the ends of triple-helix peptides to the Au NPs to form a unit cell for the cube microcrystal. As Au NPs with streptavidin on the surface bind the biotinylated triple-helix peptides, we anticipate the size ratio between the triple-helix peptide and the Au NP is important to define the shape of the unit cell of the peptide nanowires.

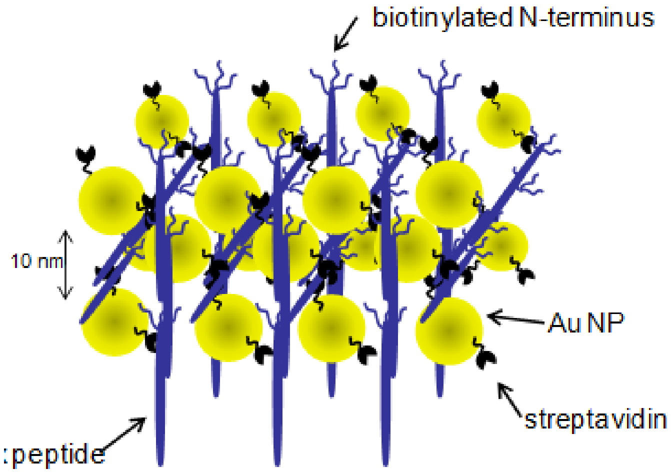

Figure 2-5: One of the proposed 3D super lattice structures of the biotinylated triple-helix peptides and streptavidin-functionalized Au NPs assembled by the streptavidin–biotin interaction.

2.4 Result and Discussion

2.4.1 Transmission Electron Microscopy (TEM)

When 10 nm diameter Au NPs decorated with six streptavidin molecules were incubated with the biotinylated triple-helix peptide in solution for one hour, the peptides were assembled into a cubic structure (Figure 2-6a). The yield of 1–2 mm cubes was extremely high with respect to uniformity in shape and dimension of the crystals, as seen in this TEM image. When the TEM grid of the sample was tilted, the edges of the cubes become visible, indicating that these cubic assemblies are three-dimensional (Figure 2-6b inset).

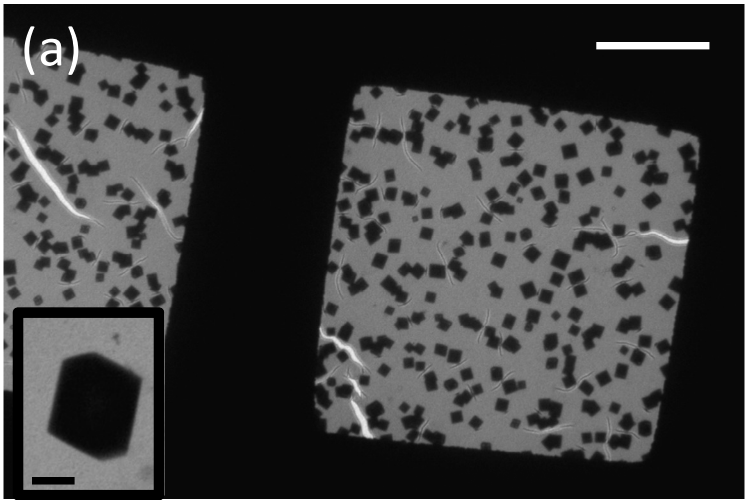

Figure 2-6: TEM image of the cubes assembled from the biotinylated triple-helix peptides and streptavidin-functionalized Au NPs. Scale bar: 20 mm. Inset: A tilted TEM image of the cubes in (a). Scale bar: 1 nm.

2.4.2 High-Resolution TEM (HRTEM)

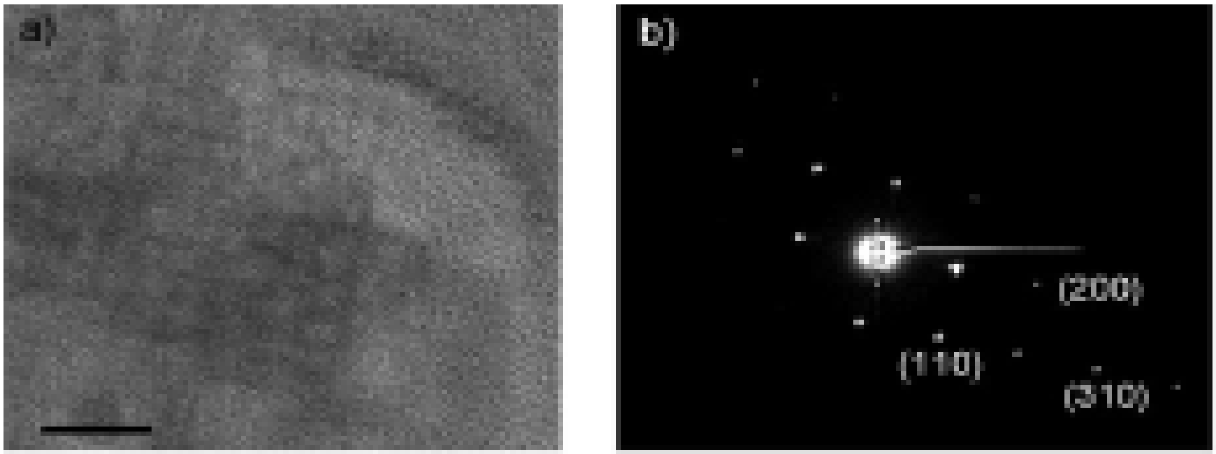

Figure 2-7: a) High-resolution TEM image of the cube assembled from biotinylated triple-helix peptides and Au NPs. Scale bar: 30 nm. b) An electron-diffraction pattern of the cube.

In Figure 7a, high-resolution TEM (HRTEM) of the peptide cube reveals that the array of Au NPs with lattice fringes and crystalline faces of Au NPs are oriented in the isotropic direction. In this image, the periodic alignment of Au NPs and the peptide frame are visible when the peptides were stained by ammonium molybdate to increase the contrast of the peptide lattice in the cube. Electron diffraction of this cube (Figure 2-7b) matches the diffraction pattern of the single-crystalline gold, indicating that the crystalline orientation of Au NPs in the peptide frame is aligned in an isotropic direction (HRTEM image in Figure 2-7a). It should be noted that the same streptavidin functionalized Au NPs mixed with non-biotinylated triple helix peptides did not produce any peptide–NP aggregations, demonstrating the crucial role of the biotin–streptavidin interaction for the assembly of the cube shaped microcrystals. Previously, mesocrystals of calcium carbonate were observed to undergo the oriented assembly to form single crystals by dipolar interactions with polymer adsorption, and the NP alignment in an isotropic crystallographic direction in this peptide–Au NP cube could also be originated from the dipole interaction of peptides and NPs.

2.4.3 Small Angle X-ray Scattering (SAXS)

Figure 2-8 shows the small-angle X-ray scattering (SAXS) pattern of the cubes measured at 30°C,with diffraction peaks located at q = 0.06, 0.11, and 0.18A^{-1}, respectively. The qx/q1 ratios of these peaks are 1:2$^{1/2}$:3$^{1/2}$, thus matching the characteristic diffraction pattern of a body centered cubic structure. On the basis of this SAXS spectrum, the interparticle distance of Au NPs in the diagonal direction of the body-centered cubic unit cell is 7 nm. A characteristic sharp increase in the scattering at small value of q in the SAXS profile indicates the long-range order of Au NPs in the cubes.[71]

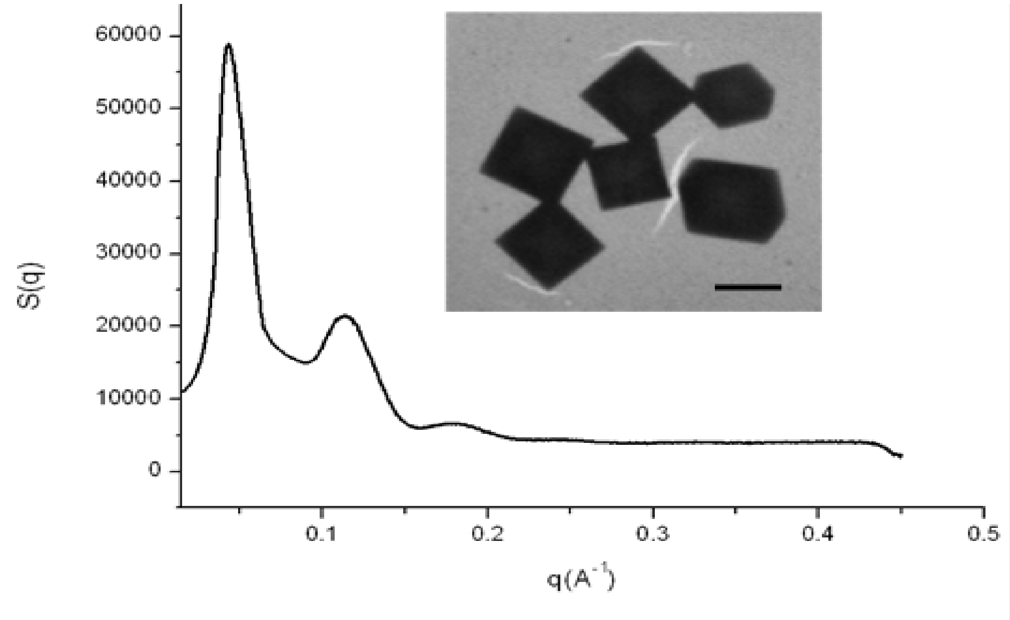

Figure 2-8: SAXS pattern of the cubes. Scale bar (inset): 2 μm.

Peak	q(Å^{-1})	distance(Å)	ratio	(*hkl*)
1	0.044	143	1	(110)
2	0.062	101	$2^{1/2}$	(200)
3	0.076	83	$3^{1/2}$	(211)
4	0.11	57	$6^{1/2}$	(222)
5	0.18	34	$18^{1/2}$	(310)

Table 2-1: BCC structural parameters for the cube obtained from the SAXS profile.

We proposed different models to explain the arrangement of nanoparticles and the peptides in the BCC structure. Figure 2-9 shows the inter layer approach of alignment of peptide joining two different layers in a unit cell diagonally. The top view in this model depicts the peptide coming towards the viewer.

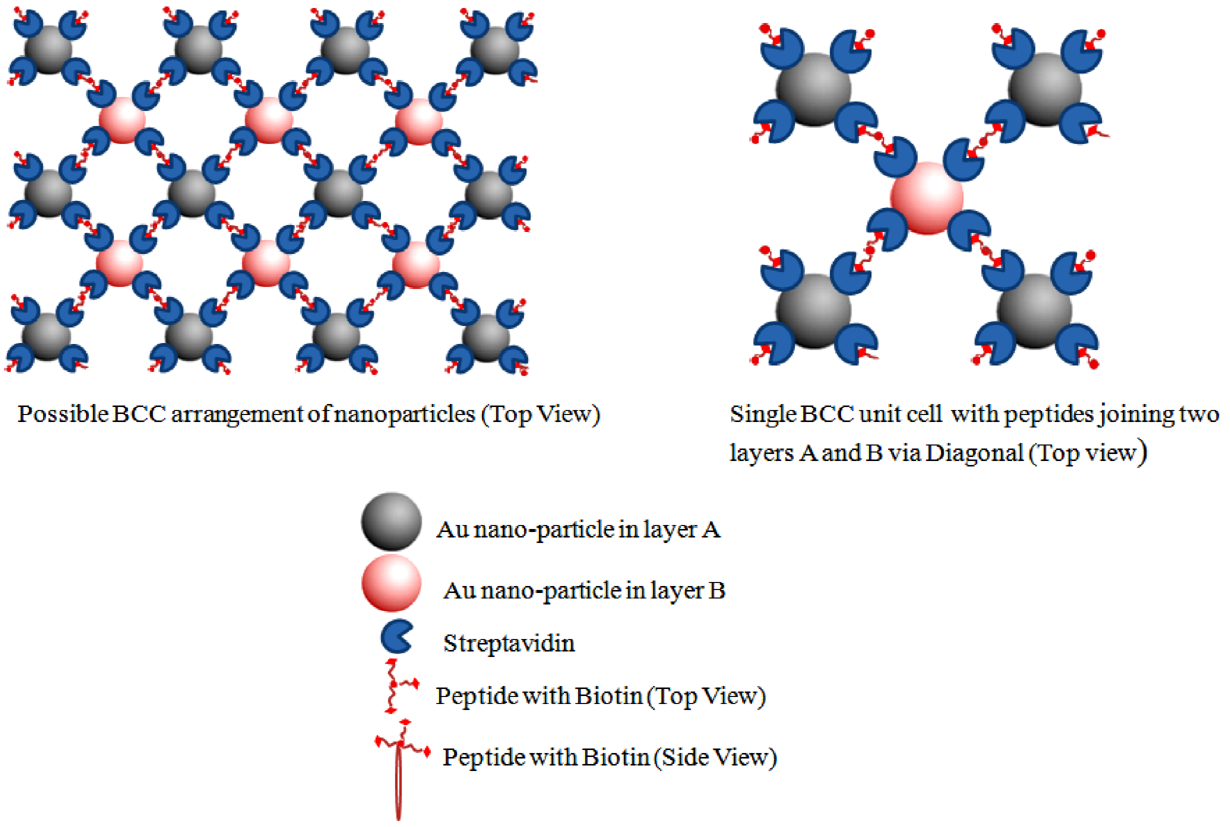

Possible BCC arrangement of nanoparticles (Top View)

Single BCC unit cell with peptides joining two layers A and B via Diagonal (Top view)

Figure 2-9: Inter layer approach for the arrangement of the peptides and nanoparticles in BCC structure.

Figure 2-10 shows intra layer approach of arrangement of the peptides and nanoparticles in BCC structure. The peptide connects A-A layers and B-B layers as shown below.

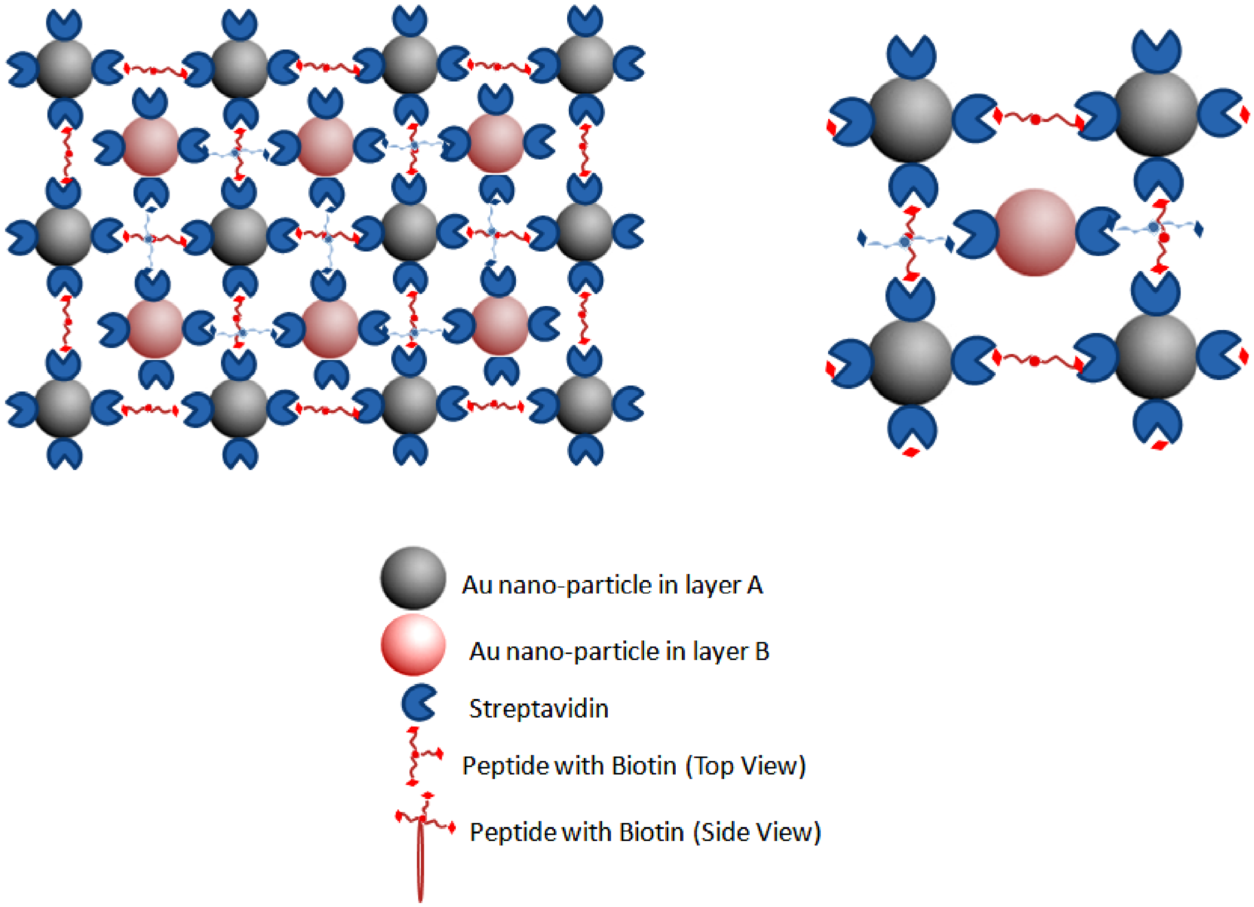

Figure 2-10: Intra layer approach for the arrangement of the peptides and nanoparticles in BCC structure.

2.4.4 Monitoring the assembly process in solution by ultraviolet-visible spectroscopy (UV-Vis)

To study the nature of assembly of functionalized gold nanoparticles and the peptide, we monitored the SPR bands with time by collecting spectra every 10 min on a sample with a relative concentration of 1:2 nanoparticles: peptide. Broadening and red shift was observed which indicates the formation of bioconjugates.[72.73] Figure 2-11 reveals that a major red shift appears to be clearly visible at 60 minutes.

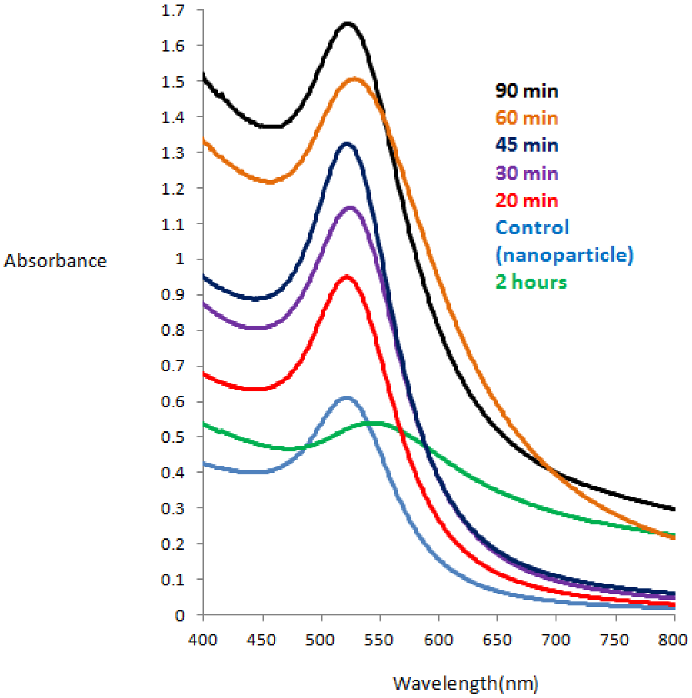

Figure 2-11: UV-Vis absorption spectra of the BAP877 and streptavidin bound old nanoparticles at different time intervals at pH 7.4.Control shows the characteristic absorbance of gold nanoparticle at 520nm.

As the assembly proceeds, the absorption decays with time after 1 hour suggesting that both components are being incorporated into the composites that precipitates over time.

2.4.5 Dynamic Light Scattering (DLS)

To further confirm if the assemblies were actually forming in solution and not during the drying process on the TEM grid, dynamic light scattering (DLS) measurements were performed on the peptide-nanoparticle samples before and after the assembly. DLS data shows that the hydrodynamic diameter of the assembled micron size complex (138nm) is much greater than that of only the peptide (7.02nm) and nanoparticles (17.2nm) which signifies that the composites are formed in the solution and not the result of solvent drying.

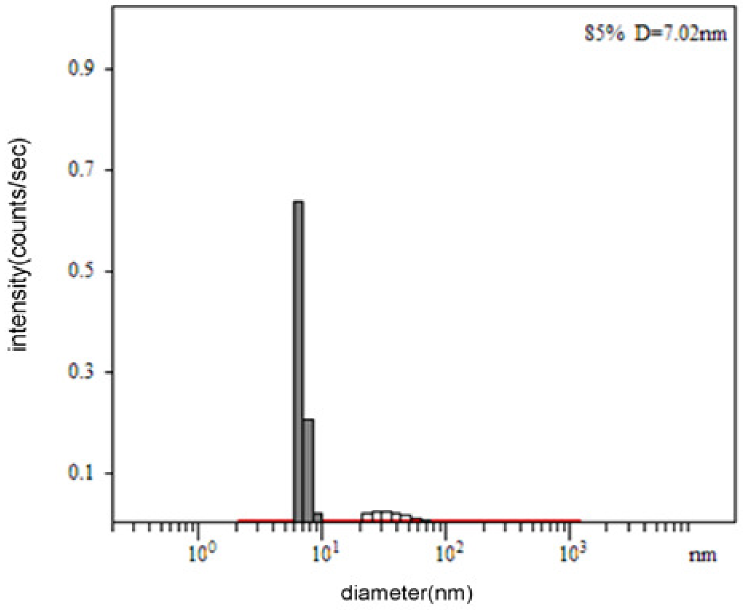

Figure 2-12: Hydrodynamic diameter of the peptide (BAP877) as measured by dynamic light scattering (DLS) before the assembly.

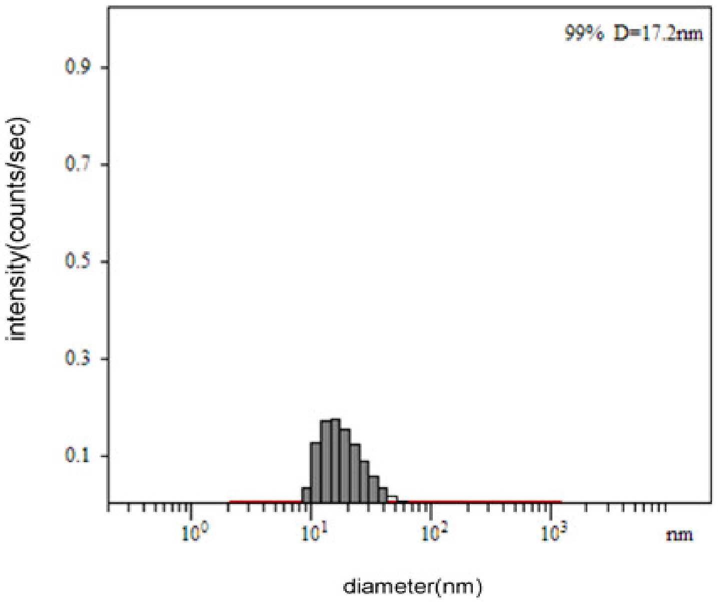

Figure 2-13: Hydrodynamic diameter of the streptavidin bound gold nanoparticles as measured by dynamic light scattering (DLS) before the assembly.

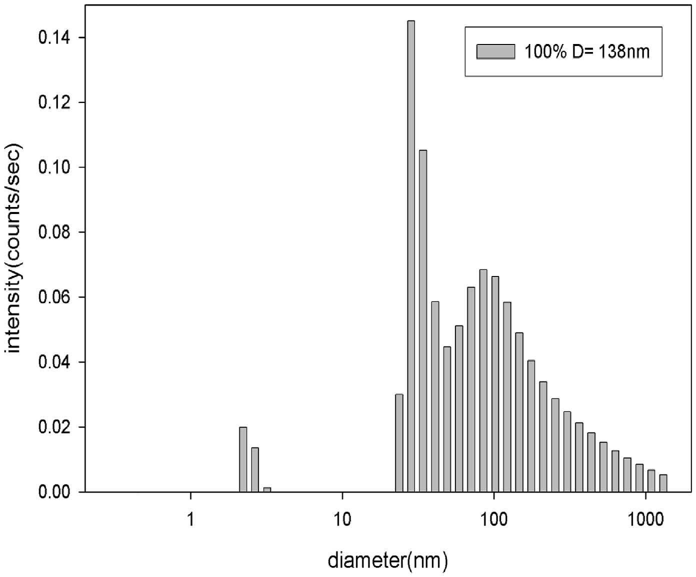

Figure 2-14: Hydrodynamic diameter of the biotin bound peptide and streptavidin ligated gold nanoparticles as measured by dynamic light scattering (DLS) after the assembly.

2.4.6 Circular Dichroism Study(C D)

A circular dichroism (CD) spectrum of these cubic superlattices indicates that the genetically engineered peptides maintain the triple-helical conformation with a small positive peak at about 225 nm and a deep negative peak at about 197 nm.

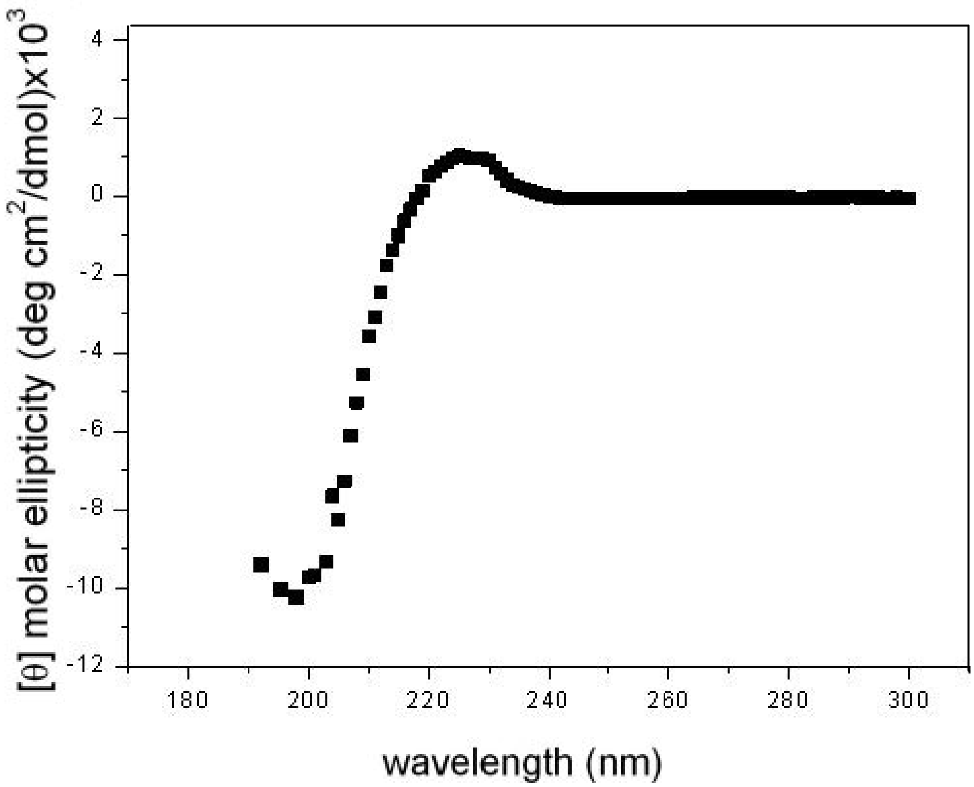

Figure 2-15: CD spectra of BAP877. The spectrum is normalized to molar ellipticity.

2.4.7 Polarized-Light Microscopy (PLM)

To further confirm the arrangement of Au NPs in the cubic peptide–NP superlattices, we also imaged these cubes by polarized-light microscopy. The contrast for the cubic crystals was diminished with cross-polarized light (Figure 2-16), supporting that the arrangement of Au NPs in the cube is isometric in the long range.

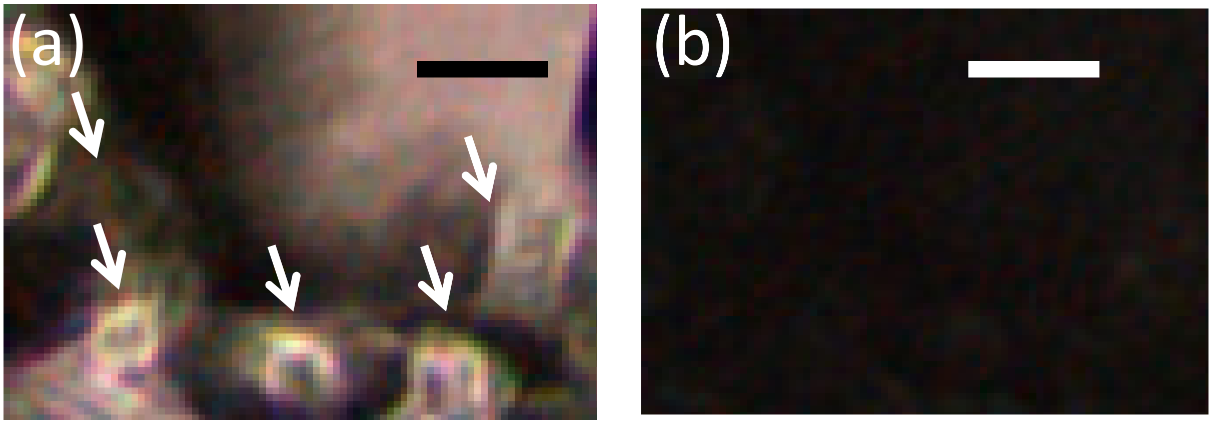

Figure 2-16: Polarized light microscopy images of the cubes (arrows) when the polarized light was applied at 0° (a) and 90° (b). (Scale bar = 3 μm).

When polarized light was applied at an angle of 0°, the optical image of the sample can be observed with high contrast, as shown in Figure 2-16a. When the light was cross-polarized (i.e., rotated at an angle of 90°), the contrast of the cubes was diminished as shown in Figure 2-16b. This result indicates that the arrangement of Au NPs in the cube is isometric in the long range.

2.5 Conclusion

In summary, we have demonstrated that a novel peptide-directed nanomaterial assembly technology could be readily presented for the construction of macroscale multicomponent materials that still retain superior nanoscale domains and properties. By applying this technique, nanomaterials can be assembled with peptides in the ordered dipole orientation and long periodicity, resulting in 3D peptide–inorganic superlattices with defined 3D shape.

The unique features of molecular recognition by peptides and large-scale 3D self-assembly enable such multicomponent 3D materials to be created in precise designs and high yields that are difficult to obtain by other templates, such as DNAs and polymers. The type of 3D peptide superlattice assembly with hybrid NP building blocks described herein shows potential to impact the future fabrication of complex 3D functional device building blocks, which demands precise long-range arrangement and periodicity of NPs. This programmable recognition based assembly provides the flexibility to modify the NP arrangement and the final crystalline structure by altering the size ratio between triple-helix peptides and NPs and/or the number of ligands on NPs, as observed in the DNA–Au NP assembly. It is also expected that more systematic investigation of the robust large-scale assembly nature of peptides on 3D microcrystal structures will provide further insight into the design and fabrication of novel 3D crystals in practical sizes.

2.6 Experimental Section

2.6.1 Recombinant Collagen as Fusion Protein for Biotinylation

The recombinant collagen-like fragment (BAP877) was generated using the original F877 bacteria expression construct [1] with the insertion of a 15 amino acid sequence of Biotin Acceptor Peptide (BAP) [2-4] at the N-terminus (Figure 2-17). The insertion of the 15 amino acids of Biotin Acceptor Peptide (BAP) was achieved by PCR using the PrimeSTAR HS DNA Polymerase (Takara Bio Inc) with the pET32a-877 (foldon) plasmid as the template and the following forward and reverse primers.

F5’GGATCCGGTCTGAACGACATCTTTGAAGCGCAGAAAATTGAGTGGC ACGAAGGTCCTCCTGGACCACCTGGG-3’.

R 5’-GGATCCGCCACAGCACGGACCTG-3’.

The fusion protein was sub-cloned into the pCR4 blunt TOPO (Invitrogen, Carlsbad, CA) plasmid and the sequence was verified by DNA sequencing (ABI PRISM 3100- Avant Genetic Analyzer, Applied and Biosystems, Carlsbad, CA).

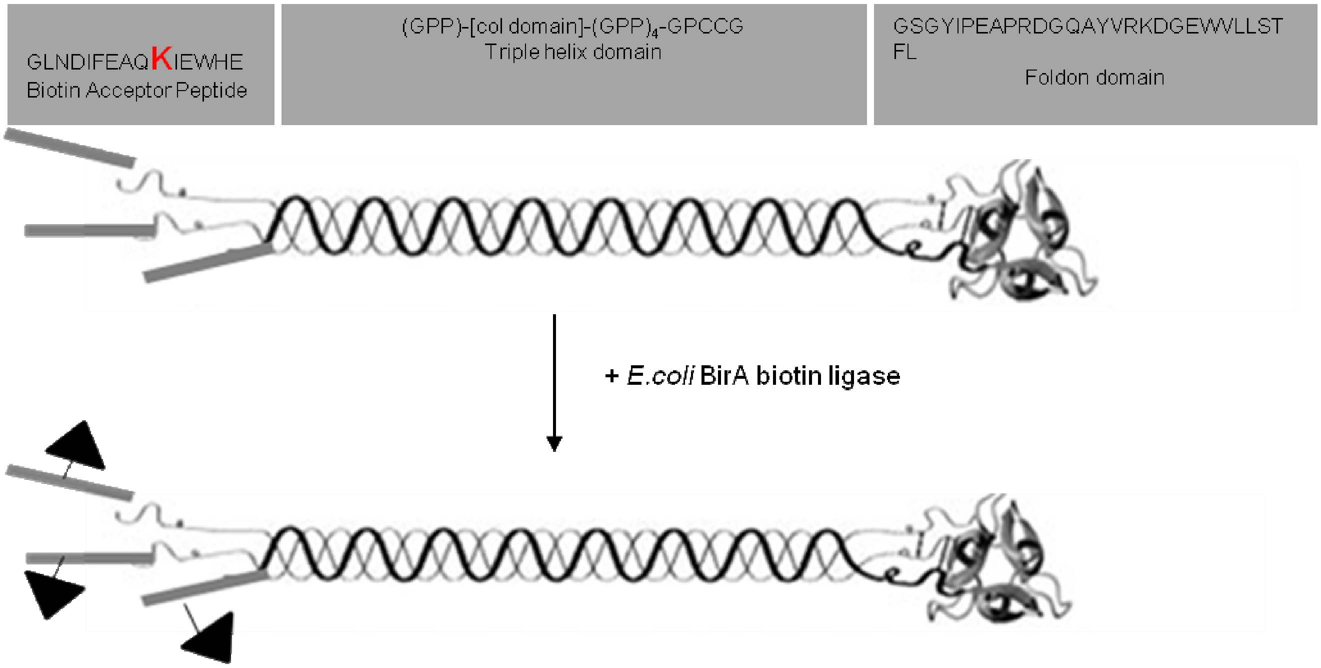

Figure 2-17: Scheme for the specific biotinylation of Biotin Acceptor Peptide (BAP) by BirA biotin ligase. The lysine (K) amino acid highlighted in red indicates the residue that is specifically biotinylated by BirA. The amino acid sequence of BAP, triple helix, and the foldon domain is shown in the box. The black triangles depict the attachment of biotin as the final step in the expression of fusion protein which can vary from 1 to 3 from batch to batch protein purified.

2.6.2 Expression and Purification of Recombinant Protein from E. coli

The constructed plasmid was transformed into chemically competent E. coli BL21 (DE3). The transformed cells were grown in TPP media (20g/L typtone, 15g/L yeast extract, 8g/L NaCl, 4g/L Na2HPO4, 2g/L KH2PO4) with 1% glucose and 50µg/ml ampicillin to OD600 of 1. Expression was induced by adding 0.5mM isopropyl-b-D- thiogalactoside (IPTG) followed by incubation at 25°C for 4–5 hrs. Cell pellets were harvested by centrifugation, and resuspended in lysis buffer (50 mM Tris-HCl pH 7.0 and 300 mM NaCl). Cell suspensions were incubated for 30 min at 4°C in the presence of 20 mg/ml lysozyme (Sigma, St. Louis, MO, USA), 1 mg/ml DNase I (Roche Molecular Biochemicals, Indianapolis, IN, USA), 100mM PMSF, (Roche Molecular Biochemicals), lysed by freeze-thaw cycles and sonication. Following centrifugation, the protein in the supernatant was purified using nickel affinity chromatography according to the native purification protocol provided by the manufacturer (Ni-NTA Superflow; Qiagen, Valencia, CA, USA). The Ni-NTA column was washed with buffer containing 10 mM imidizole and eluted with buffer containing 300 mM imidizole. The 6X His and thioredoxin tag was cleaved using Thrombin Clean cleave Kit (Sigma) overnight at room temperature. The final protein was purified by RP-HPLC (Beckman Coulter) with C18 column (Vydac) with a 20-70% acetonitrile –water with 0.1 % TFA (Figure 2-18). The peptide elution peak was collected, lyophilized, stored at -80°C. The expression level and purity of the sample was assayed qualitatively by sodium dodecyl sulphate polyacrylamide gel electrophoresis (SDS-PAGE) (Figure 2-19). BAP877 peptide is a monodisperse nanowire with a mean length of 42 nm (Figure 2-4). Circular dichroism (CD) spectrum of BAP877 at 4°C indicates that the genetically-engineered peptides maintain the triple helical conformation with a small positive peak at ~225nm and a deep negative peak at ~ 197nm (Figure 2-15).

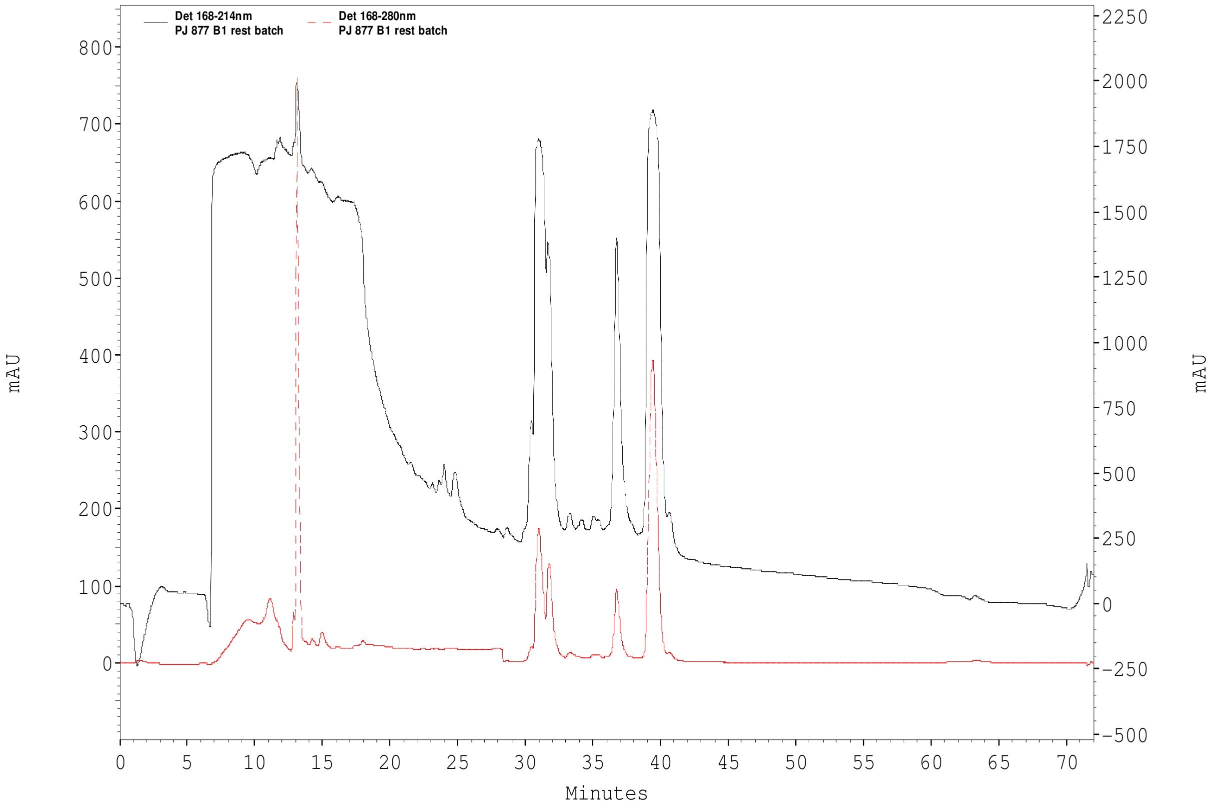

Figure 2-18: High-Performance Liquid Chromatography (HPLC) of BAP877 (HPLC absorbance at 280 nm (black) and 220 nm (red)). The peak for the pure protein appears at an absorbance of 280nm.The arrows 'a' and 'b" correspond to the peaks of pure protein and thioredoxin after thrombin cleavage, respectively.

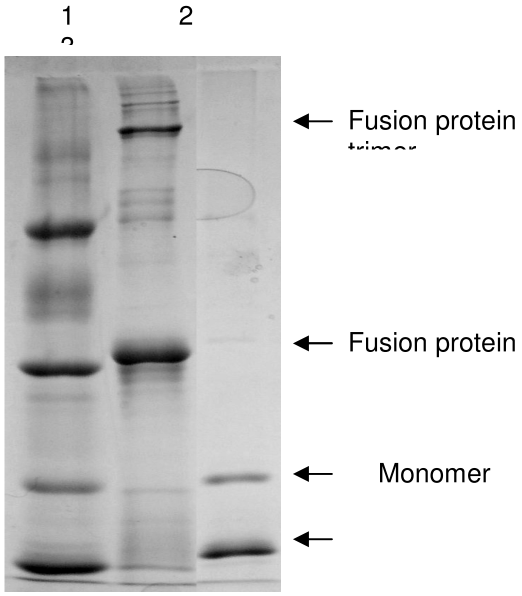

Figure 2-19: SDS-PAGE analysis of the expression of BAP877. Lane 1: Protein molecular weight marker (66kD, 45kD, 36kD, 29kD, 24kD, 20kD, D). Lane 2: Purified protein by Ni-NTA affinity column, Lane 3: After thrombin cleavage.

2.6.3 Biotintylated BAP877

Gold nanoparticles with bound streptavidin were purchased from Nanocs (New York, NY). The diameter of the gold nanoparticles is 10 nm. The density of streptavidin is 4 to 6 per Au NP. The conjugated nanoparticle solution was diluted to 1:10 with 0.1mM HEPES (pH 7). Before the reaction was carried out, the lyophilized protein was brought up in phosphate buffered saline (PBS) (pH7.5). After the diluted streptavidin-gold conjugate was allowed to equilibrate for 30 min at room temperature, biotinylated BAP877 (10 mg/ml) was incubated in the molar ratio of 1:2 for 1 hr at 4°C. TEM images of all samples were obtained with the same drying time on the grid and all the steps in the reaction and their imaging was carried out on the same day.

2.6.4 Transmission Electron Microscopy (TEM)

A drop of the Au NP-peptide sample (4 μl) was applied to a carbon- coated copper TEM grid (Electron Microscopy Sciences, PA) and dried with filter paper. The sample was stained with filtered 0.5% ammonium molybdate and examined by TEM and electron diffraction (JOEL 1200 EX) at 100KV. For high resolution TEM imaging, an acceleration voltage of 200 KV was applied with a JOEL JEM-2100 LaB6 TEM.

2.6.5 Small-Angle X-ray Scattering (SAXS)

The SAXS experiments were performed on the Bruker X- ray instrument at the Center for Advanced Technology in Photonics Application (CAT) at the City University of New York, with X rays of wavelength 1.54 A° (50 kV). Aqueous samples were first dried using nitrogen followed by vacuum drying for 7 days, and the solid samples were placed between Alumina foil windows for irradiation with a 1×1mm2 beam. The scattered radiation was detected with a VANTEC area detector. The magnitude, q, of the scattering vector is $4\pi\sin\theta/\lambda$, where $2\theta$is the scattering angle and λ is the wavelength of the incident radiation. All the SAXS data were corrected for sample transmission, background and detector sensitivity respectively. The 2D scattering data was azimuthally averaged and the resulting 1D profiles of the scattered intensity as a function of the scattering angle, 2θ, were altered into profiles of scattering intensity with silver behenate as a standard. The SAXS profile in Figure 2-20 was converted to structure factor and fitted into Gaussian profiles to obtain the peak position, area, height and width as shown in Table 2-2, and the structure parameters of the cube match B.C.C structure with the lattice parameter of 20 nm and the interparticle distance of 7 nm to the nearest neighbors .

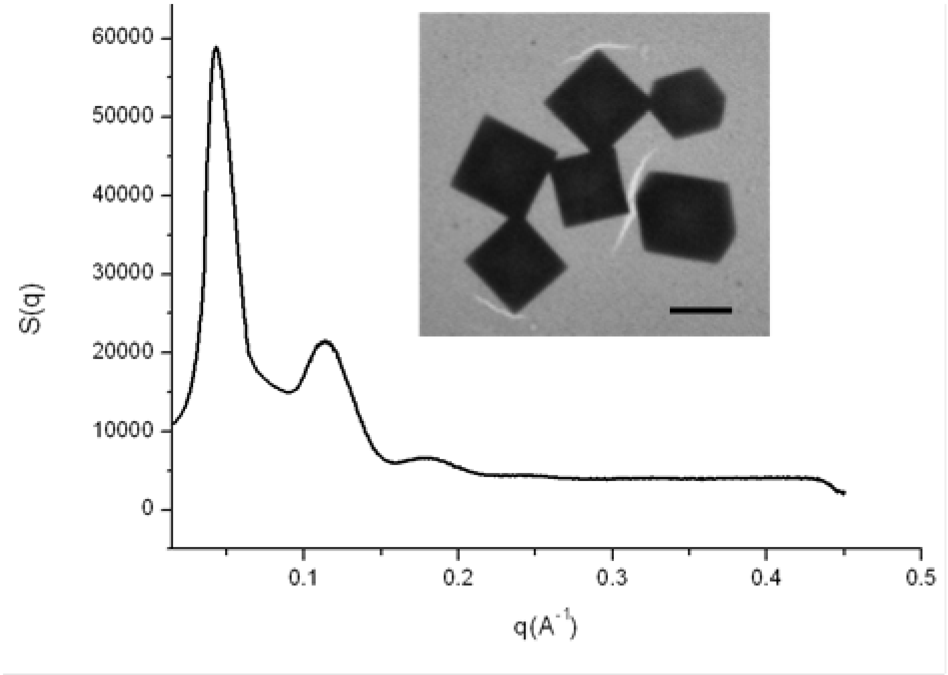

Figure 2-20: SAXS pattern of the cubes. Scale bar (inset): 2 µm.

Peak	q(Ǻ$^{-1}$)	distance(Ǻ)	ratio	(*hkl*)
1	0.044	143	1	(110)
2	0.062	101	$2^{1/2}$	(200)
3	0.076	83	$3^{1/2}$	(211)
4	0.11	57	$6^{1/2}$	(222)
5	0.18	34	$18^{1/2}$	(310)

Table 2-2: BCC structural parameters for the cube obtained from the SAXS profile.

2.6.6 Dynamic Light Scattering (DLS)

Dynamic light scattering (DLS) measurements were performed by using Zetasizer Nanoseries ZS (Malvern Instruments) containing a He-Ne laser operating at an incident wavelength of 652nm.

CHAPTER 3: pH AND SALT DEPENDENT STUDIES ON CUBIC CRYSTAL

3.1 Introduction

In order to build a functional device by assembling materials, one has to recognize whether the nature of the interaction between the particles is weak, strong, or reversible. Research groups have studied the assembly of gold nanoparticles with temperature[74-76], biomolecular interaction, and pH. The main factor governing the assembly is the pH of the medium and there have been many reports on the configuration of the reversible assembly of gold nanoparticles induced by pH.[77-81]

3.2 Effect of pH on Peptide Directed Nanoparticle Cube Formation (from peptide's [BAP877] perspective)

To understand the role of pH on cube formation, we studied this effect based on the BAP877 (triple helix) assembly at various pH conditions. The important forces that stabilize the collagen involve both covalent and noncovalent interactions.[82] The noncovalent interactions, specifically the electrostatic forces, and the hydrogen bonding are important for maintaining the molecular structure of collagen.[83]

The ionic interactions in the form of salt bridges are the long range interaction and the maximum stability is observed when both acidic and basic residues are ionized because of the formation of intra and inter chains favorable ion-pairs[84-91]. The high dielectric constant of the solvent has been confirmed to effect the stability of the proteins by altering the ionic strength of the meduim.[92-93]

The effect of pH on the stability of collagen has been studied based on the tensile strength. It is defined as the maximum force exerted on the material to the point where it breaks apart.Much of the tensile strength of the collagen comes from the crosslinking of the fibrils to form fibers. The loss of tensile strength under acidic conditions is attributed to the cleaving of the acid sensitive inter molecular cross links. [94-95] Studies on model collagen-like peptides reveal that the triple helical conformation of peptide is stable depending on the pH range due to formation of inter and intrachain ion pairs where a set of $(\text{Gly-X-Y})_n$ peptides containing a small number of charged residues were studied showing that the triple helcial conformation is stable over a wide pH range, making it feasible to alternate charges on these ionizable groups by pH.[90]

Studies carried out by Xu's group on the triple helix (F877) have demonstrated that unfolding is caused by the interruption of a set of interchain salt-bridges formed between the Lys and Glu residues of a KGE sequence. Such interchain salt bridges are known to stabilize short peptides. Their data highlighted the critical role of the long range impacts of salt bridges in modulating the stabilities of the neighboring region of the triple helix by mutating the residues involved in salt bridge formation in the model systems.[96] When the pH is lowered, the interaction beween these charged groups is disrupted and break the salt bridges which decreases the stabiity of the triple helix.[97-98]

GSGLNDIFEAQKIEWHEGPPGPPGPPGPPGPPGPPGPVGPAGKSG DRGETGPAGPAGPVGPVGARGPAGPQGPRGDKGETGEQGDRGIKGH RGFSGLQGPPGPPGPPGPPGPCCGGSGYIPEAPRDGQAYVRKDGEWV LLSTFL

Figure 3-1: Amino acid sequence of BAP877 peptide

The study done by Willett et al.[99] suggests that the electrostatic charge of the peptides may play a role in the binding affinity toward various materials. Tang and coworkers demonstrated that peptide nanofibril template can assemble arrays of nanoparticles through electrostatic interactions. The structure was further controlled by pH and the size of nanoparticles.[100] This outcome motivated us to study the assembled structure of the B877 peptide and functionalized Au NPs with pH and NP size changes.

Therefore, for understanding the role of pH in the peptide-NP cube formation, we first measured the thermal stabilities and the assemby of peptide-nanoparticle at different pH.

3.2.1 Result and Discussion

3.2.1.1 Zeta Potential of the B877 peptide (Determining the isoelectric point-pI)

Iso electric point (pI) is the point where the surface charge on the molecule is zero. In case of protein, at pH below the pI, protein carries a net positive charge and at the pH above the pI the net charge is negative. The overall charge on the peptide is determined as a function of pH (Figure 3-2).

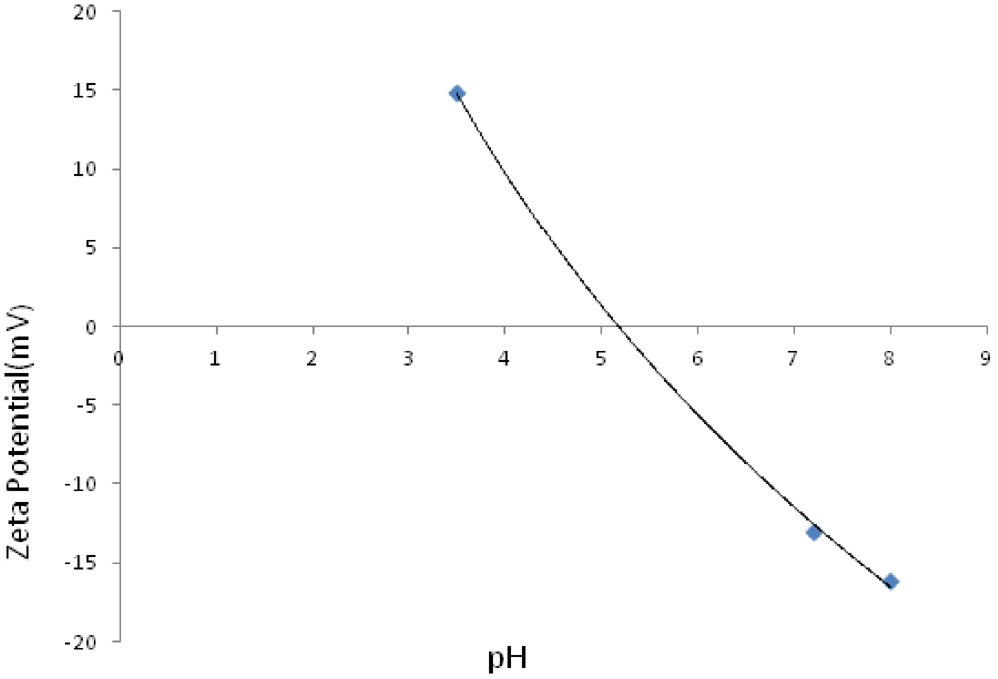

Figure 3-2: Plot of zeta potential with pH for BAP877 peptide

pH	**Zeta Potential(mV)**
3.5	14.88
7.04	-13
8	-16
7.2(0.2M NaCl)	-11.5

Table 3-1: The corresponding zeta potential values at a given pH

3.2.1.2 TEM Studies

To understand the pH effect on the BAP877 peptide aggregation/assembly, control experiments were carried out to examine the assembled structures of peptide with pH change without using Au NPs.

Figure 3-3 shows TEM micrographs of BAP877 (peptide) samples at different pHs. The peptides show the typical dispersed rice-like structure of peptide nanowire at all pH with the secondary structure typical of triple helical protein as confirmed from cirular dichrosim.

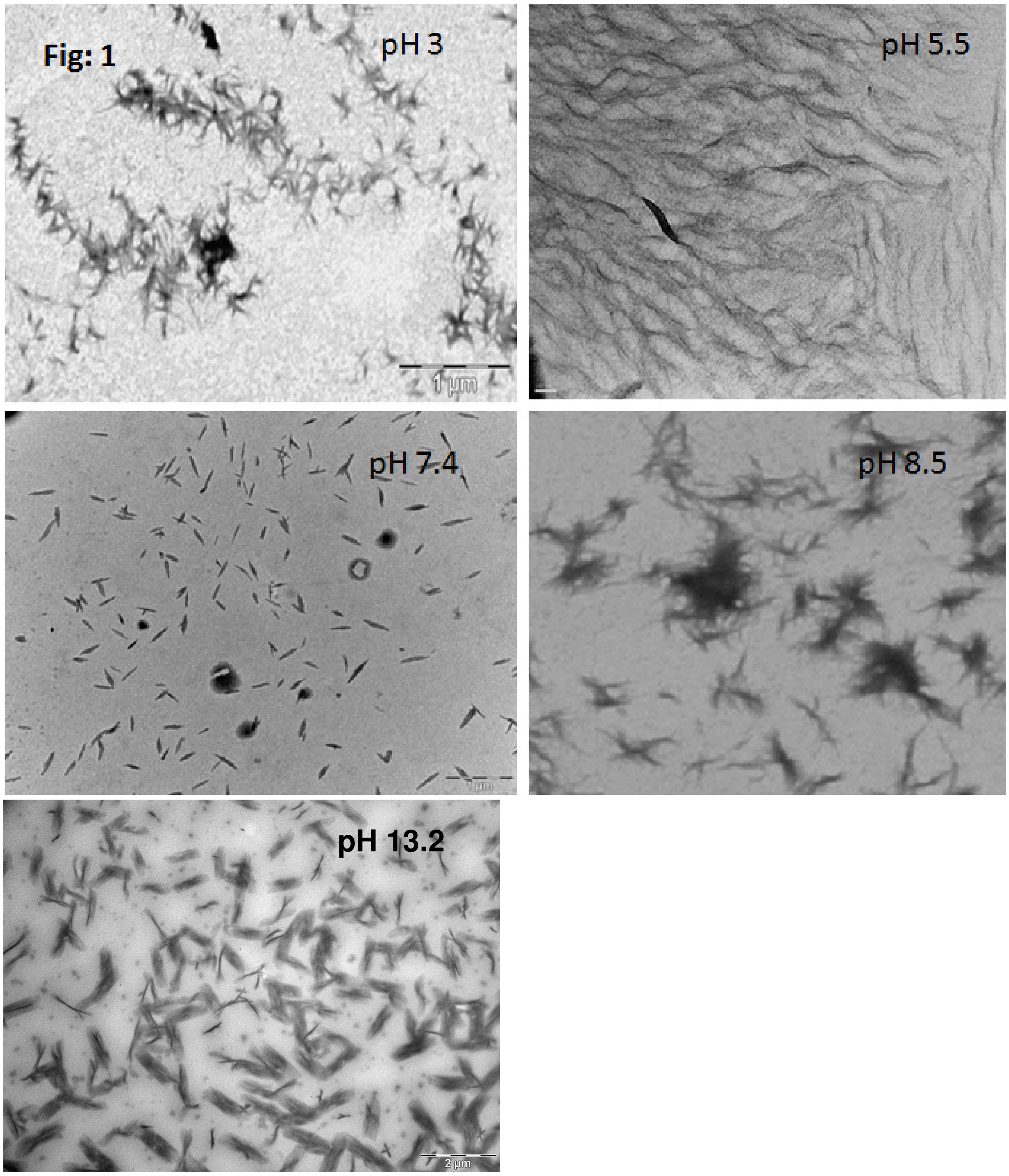

Figure 3-3: TEM images of BAP 877 at pH 3, 5.5, 7.4, 8.5 and 13.2.

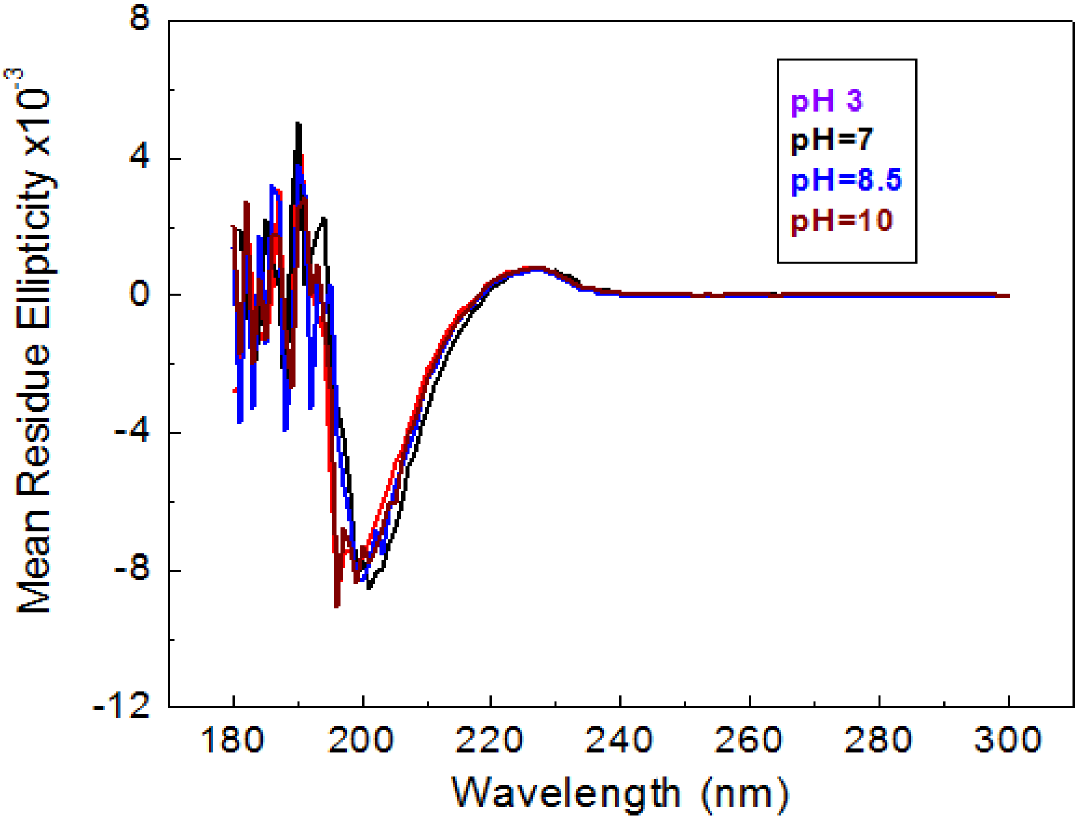

Figure 3-4: CD spectra of BAP 877 at pH 3, 5.5.7.4 and 8.5 were taken at 4° C

The CD spectra is shown in Figure 3-4, at all pH values examined, the peptide has a CD spectrum with the characteristic small postive peak at ~ 225nm and a deep negative peak at ~ 197, identical for the triple helix conformation.[101-102] This means that charge present on the peptide at different pH affects the local conformation but does not disrupt the secondary structure (the triple helical conformation).

3.2.1.3 Melting Temperature Curves

The temperature of thermal transition (T_m) which measures the stability of the peptide with temperature was determined as a function of pH, monitored by the change in the CD signal at 225 nm with temperatures from 4°C to 70°C. The temperature of thermal transition (T_m) for BAP877 at pH 7.4 is around 40 °C higher than acidic pH values (T_m< 35°C) as shown in Figure 3-5 .

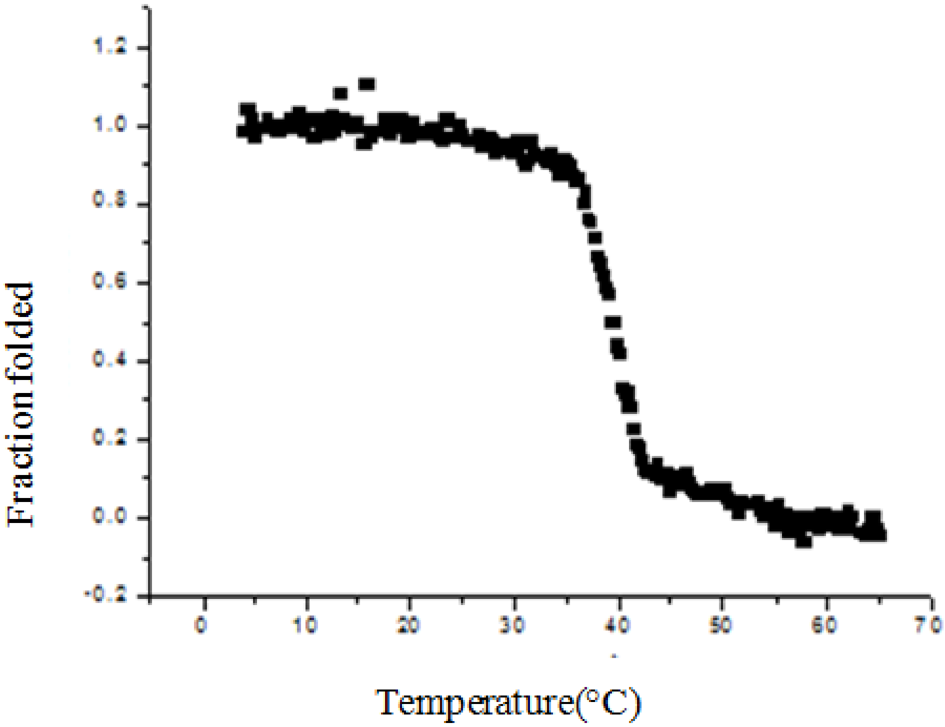

Figure 3-5: Melting temperature curves of BAP 877 at pH 7 by monitoring the peak intensity at 225nm in CD spectra.

At pH 7.4, T_m for BAP 877 is around 40 °C, relatively higher than the wild type collagen (37°C) [103] due to the repeating Gly-Pro-Pro sequences, the Cys-knot and the foldon (T_m ~70°C).[104] The stability of the peptide is lower at acidic pH 3, (T_m < 35° C) Figure 3-6. The high stability of the triple helix at elevated temperature makes it robust biomaterial that can be used as a template for bio fabrication.

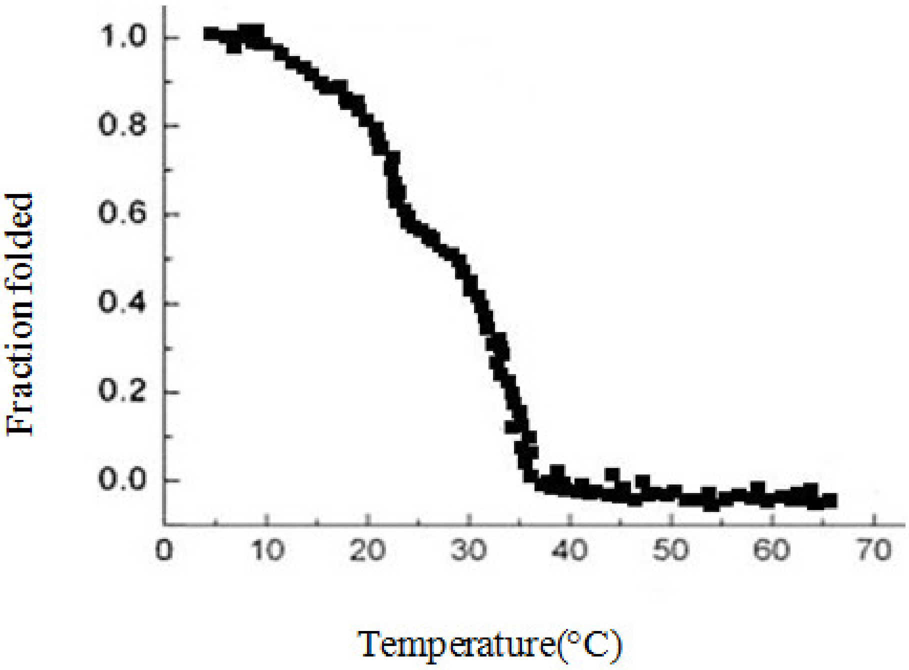

Figure 3-6: Melting temperature curves of BAP 877 at pH 3 by monitoring the peak intensity at 225nm in CD spectra.

3.2.1.4 Assembly Study of BAP877 Peptide and Au Nanoparticles

At highly acidic (pH 3) and basic conditions (pH 13.2), the assembly of BAP877 peptide and Au NPs did not result in cubic crystals (Figure 3-7) .There is an interplay of various forces like the repulsive forces which are dominant at extreme pH conditions, electrostatic interactions, apart from the vanderwaals and hydrophobic forces. At this stage, we cannot predict the role of each force that affect the crystallization process at this pH, but we can only hypothesize that the range of effective interactions depends on the pH and salt concentration of the medium.

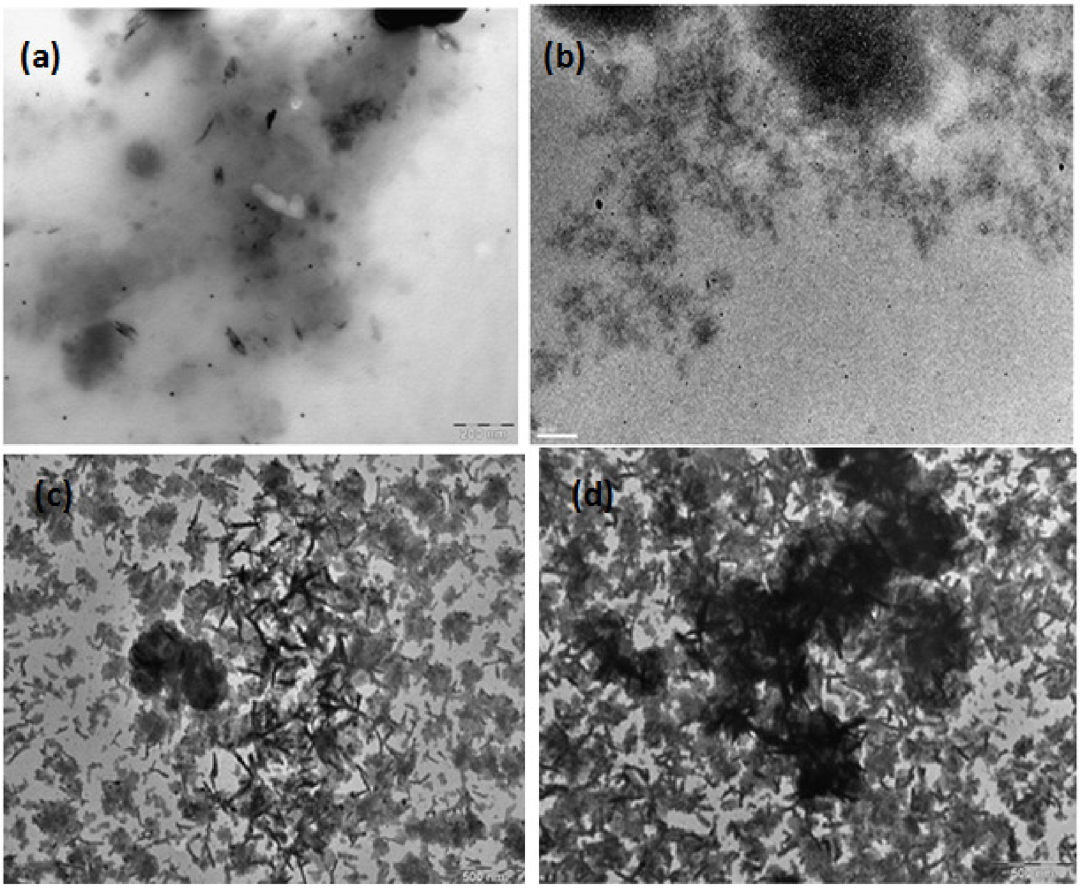

Figure 3-7: TEM images of the assembly of the BAP877 and streptavidin gold nanoparticles at(a), (b) pH 3 and (c), (d) pH 13.2at 4 °C

At pH 8.5, BAP877 peptides and Au NPs are assembled into cubic structure as shown in Figure 3-8. This behavior is typically observed in the non classical pathway of crystallization as explained by Frenkel.[105] The ions in this pH and salt concentration mediate the long range interaction but induce the short range interaction of the large proteins. As we pointed out before, there may be other effective interaction that is modulating this pathway but we can only speculate at this stage that pH 8.5 with right amount of salt concentrations is effective for mediating the range of interactions.

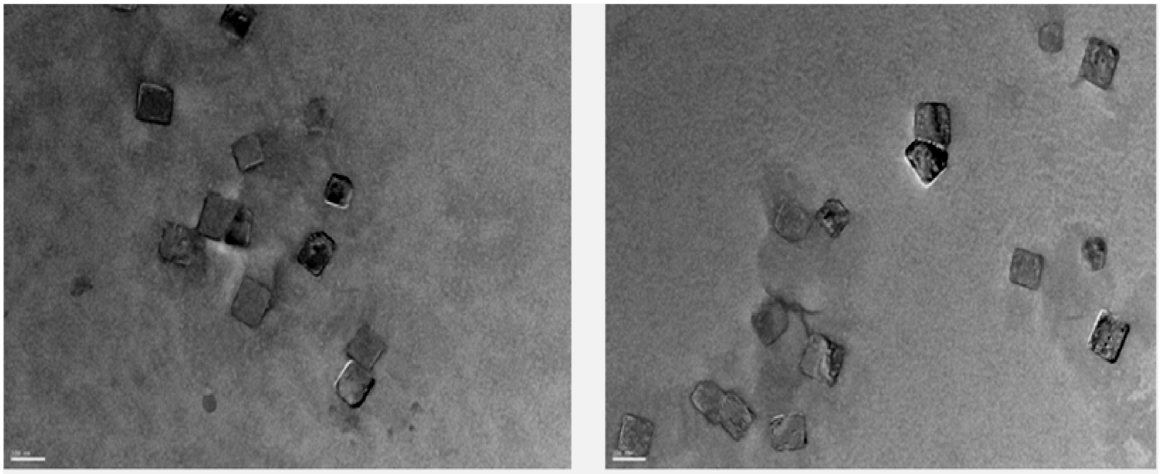

Figure 3-8: TEM images of the assembly of the BAP877 and streptavidin gold nanoparticles at pH 8.5 at 4 °C.

3.2.2 Conclusion for pH studies

For the BAP877 peptide and Au NP co-assembly, pH plays an important role in maintaining the native rod like structure of the triple helix. In acidic and basic conditions, the triple helix aggregates and cannot anchor the gold nanoparticles via the biotin-streptavidin interactions. After examining different pH conditions, we found that the optimum condition favoring the cubic crystal formation is pH 7.4 to 8.5, where the triple helix retains its rod like conformation.

Based on the different pH conditions, it turns out that the cubic crystal formation takes places at pH 7.4 and 8.5.We do not have the experimental proof to explain which force is dominant for crystallization to occur. Based on the simulation studies on proteins carried out by Frenkel, [105] long range and short range interaction is mediated by pH and salt. In our system the salt concentration and pH are right at pH 8.5 to favor the non classical method of crystallization which is not too strong interaction (classical) but not too weak so that the molecules can re-arrange to form ordered structure. In this range, the ions mediating the long range interaction, induces short range interaction for large proteins.

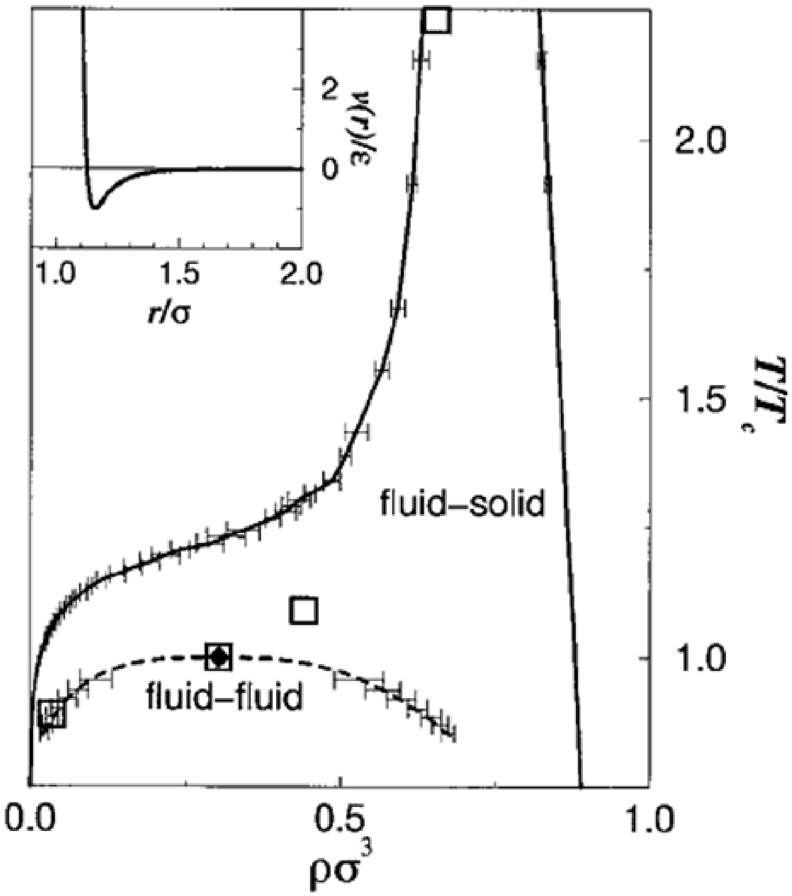

Figure 3-9: Phase diagram with short-range attraction. The diamonds indicate the fluid-fluid critical points. The solid lines indicate the equilibrium coexistence curves. The dashed curve indicates the metastable fluid-fluid coexistence (adapted from[105])

Figure 3-9 explains the non-classical pathway of crystallization[105] for short range attraction which explains that when the range of attractions is reduced by the pH and salt concentration of the solvent, two stable phases exist, solid and liquid.

Since pH control is not independent of salt concentrations at higher pH, we were interested to examine the pH dependent salt effects on the triple helix aggregation. It has long been understood the impact of salt on the stability of proteins by altering the interactions of the aqueous solvent between the proteins, known as the ‘Hofmeister effect’ as well as screening of the electrostatic interaction between the charged residues on the protein surface. The high ionic strength is known to destabilize the ion pairs. [106]

3.3 Effect of Ionic strength on Peptide-Directed Nanoparticle Cube Formation (from peptide's [BAP877] perspective)

The effect of salt concentration on the assembly of collagen has been described by different studies mentioning the role of various cation and anions in the salt modulating the stability of collagen. [107-109] Salts have significant influence on the crystallization mechanisms and the resulting crystals by changing the balance between the short range attractive and repulsive interactions takes place by tuning the surface charges with counter ions in the mixture of oppositely charged protein particles.[110-111] Different salt solutions with same ionic strength have a completely different effect on this delicate balance attractive and repulsive interaction. [112] Increase in the ionic strength of NaCl from 0 to ~ 1.02M at pH 3.7 resulted in increasing the thermal stability of collagen fibers assembly in connective tissues due to the formation of inter molecular ion pairs. [113]

The electrostatic interaction range is measured by using Debye screening length (K^{-1}) and the effect of different salts shifts the length; some salts like KCl[114] and NaCl[115] favor the formation of ion pairs to maintain the stability of the triple helix.[116]

In this part of the study, we examined the peptide-Au NP assembly under the effect of varying the NaCl concentration at pH 7.4.

3.3.1 Result and Discussion

3.3.1.1 Salt Concentration Effect on Neat Peptide Aggregation at pH 7.4

At pH 7.4, the effect of varying the salt concentration on the cube formation was studied. The optimum concentration of NaCl that resulted in the cube formation is 0.15M.[111]

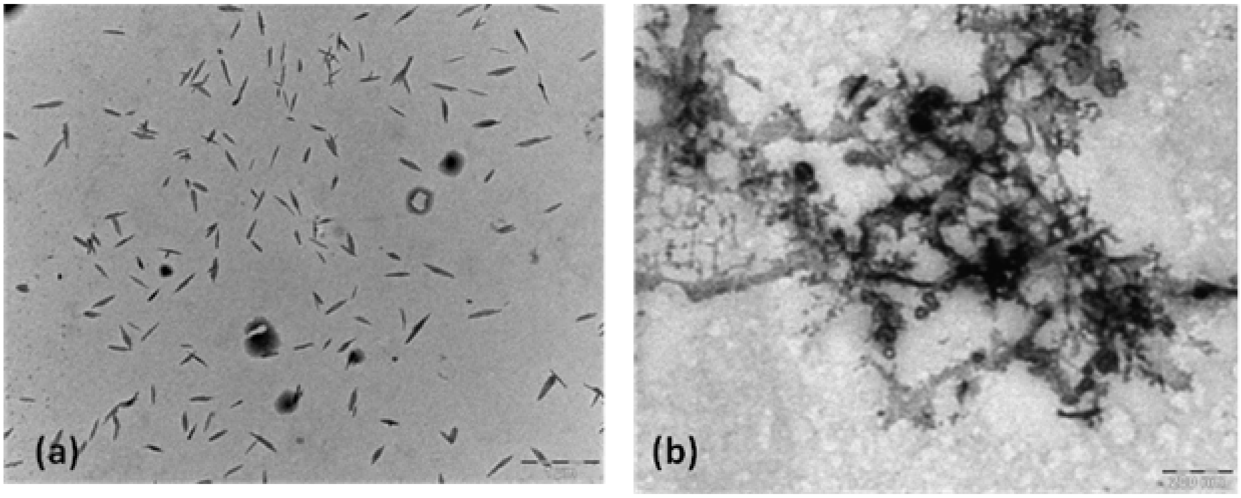

Figure 3-10: TEM images of neat BAP877 with (a) 0.15M NaCl and (b) 0.3M NaCl

At ionic strength of at 0.15 M NaCl, the neat BAP877 peptides are dispersed with the characteristic rod like/rice shape nanowires, monodisperse with length of ~ 40 nm, as shown in Figure 3-10.[117] When the NaCl concentration is increased from 0.15 M to 0.3M, the peptide aggregates due to the removal of water molecules from the peptide surface by the salt ions, which reduces the number of water molecules around the BAP877 peptide; without water molecules, exposed hydrophobic interactions coagulate the peptides.

3.3.1.2 Salt concentration effect on neat peptide aggregation at pH 3

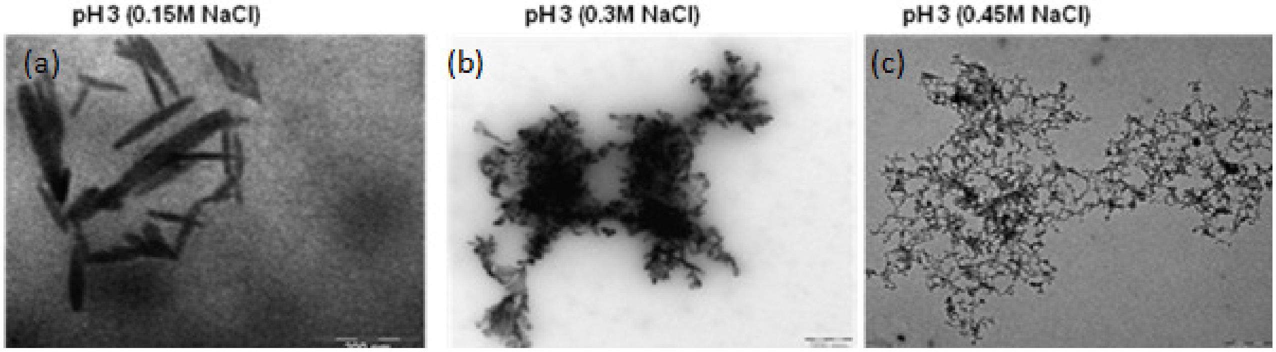

Figure 3-11: TEM images of neat BAP877 with (a) 0.15M NaCl (b) 0.3 M NaCl (c) 0.45M NaCl

At acidic pH, collagens are soluble[118], however when the concentration of NaCl is increased, the binding of anion on the peptide reduces the repulsion and expects to initiate the aggregation.[115] To examine our hypothesis that the salt concentration can indeed modulate short-range interaction between proteins to induce the assembly, before examining the BAP877 peptide – Au NP system, we studied the assembly of neat BAP877 peptides at pH 3 with different salt concentrations. From TEM micrographs shown in Figure 3-11; it clearly shows that at pH 3 with NaCl concentration of 0.15 M, the triple helix maintains its rod-like morphological structure, as expected. As the concentration of NaCl is increased from 0.15M to 0.3M, to 0.45 M, the higher NaCl concentration induces more peptide aggregation. This observation shows that the salt concentration is indeed important to modulate the assembled structure of peptides and we examine the same experiments with Au NPs in the next section.

3.3.1.3 Salt concentration effect on peptide –Au NP assembly at pH 3

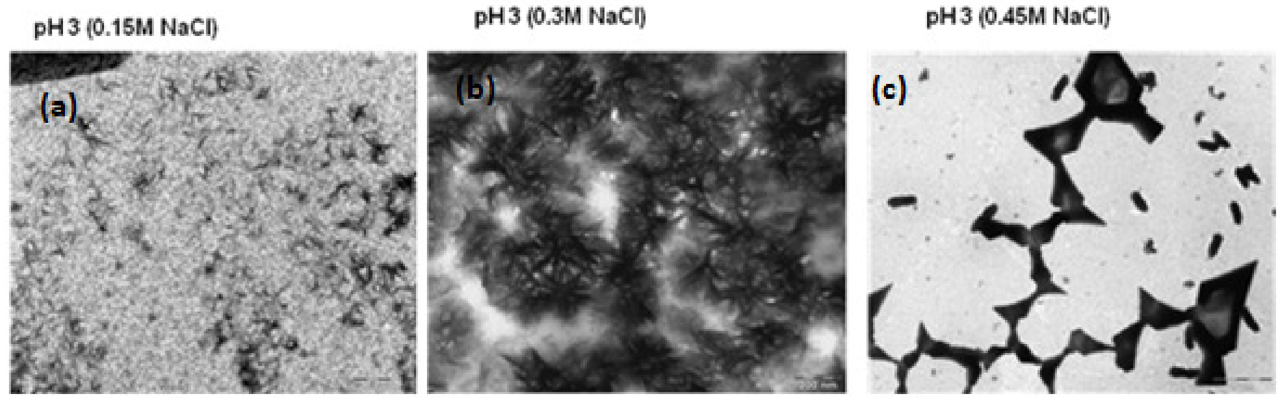

Figure 3-12: TEM images of BAP877 with streptavidin bound gold nanoparticles with (a) 0.15M NaCl (b) 0.3M NaCl (c) 0.45M NaCl at pH 3.

When the peptide is assembled with nanoparticles at pH 3 at 0.15M salt, no assembly was observed as shown in Figure 3-12. However, as the salt is increased to 0.3M, the excess positive charge on the BAP877 peptide is reduced by binding Cl^- ion on positively charged amino acids on the peptide, resulting in the aggregation as shown in Figure 3-12-(b). This trend is further observed as increasing the salt concentration to 0.45M as shown in Figure 3-12-(c).

	Low pH(3)	**Intermediate pH(7.4)**	**High pH(8.5)**
Stability of single triple helix	Less stable (protonation of COOH occurs)	Stable (formation of favorable ion pairs that forms salt bridges and inter and intra chain electrostatic bonds)	Stable (formation of favorable ion pairs that forms salt bridges and inter and intra chain electrostatic bonds)
Aggregation of triple helix	Soluble(repulsive)	Aggregates to form cubes	Aggregates to form cubes

	Low salt conc.(0.15M)	**Intermediate salt conc.(0.3M)**	**High salt conc. (0.7M)**
Stability of single triple helix	stable	aggregation	Precipitation
Aggregation of triple helix	Cubes	Random aggregation	Random aggregation

	Low salt conc.	**Intermediate salt conc.**	**High salt conc.**
Low pH	Unstable(aggregates)	aggregated (fibers)	aggregated(fibers)

Table 3-2: Summary of pH and salt concentration on neat peptide and peptide-Au NP assembly on the basis of TEM observation.

3.4 Discussion

On the basis of our experimental analysis, we have found that the optimal conditions suitable for the cubic crystal formation are highly dependent on pH and salt of the medium but the range of the growth condition for the cubic assembly is very narrow. The minimum ionic strength for effective interaction is 0.15M NaCl and range of pH is around 7.4-8.5 with lower and higher pHs leading to no cubic assembly.

The recent theory of self-assembly of nanoparticles into crystalline geometry helps explain the role of manipulation of charges to control the assembly of crystal structures. [119-120] Binary mixtures of opposite charged particles can be assembled in crystalline form when both repulsive and attractive forces (interaction energy) are balanced. This means that the surface charges on the particles have to be optimized to favor the crystal assembly. Too high intermolecular attractive interaction results in the aggregate formation which leads to amorphous precipitates. [121] To compensate the net attraction, the repulsive force needs to be introduced in the system increasing the counter ions from media like salts.

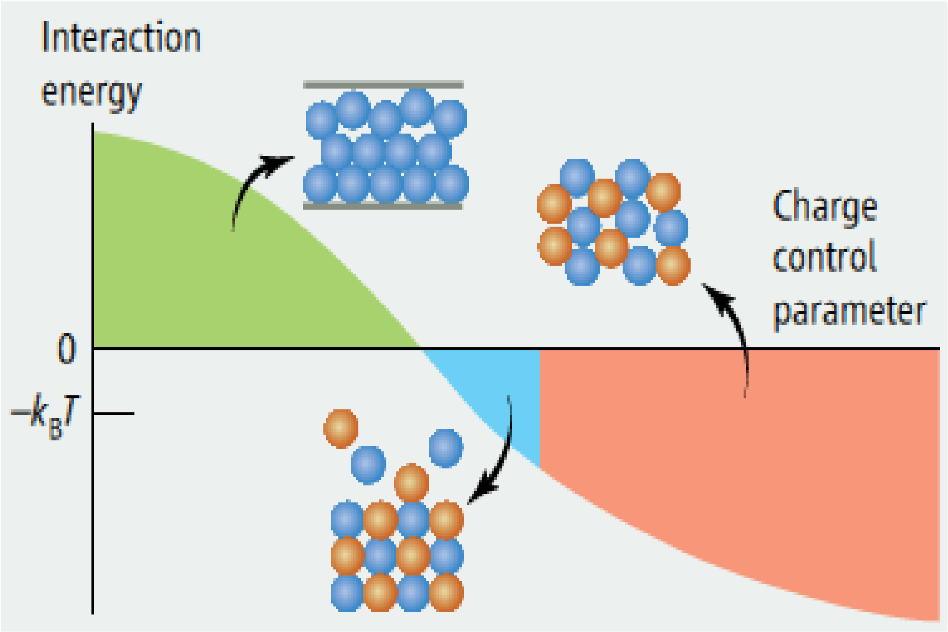

Figure 3-13: The diagram illustrating that crystallization of colloidal particles and biomacromolecules is dependent on the interactions between the particles, controlled by charge (adapted from[122])

The range of interactions can be changed by pH and salt concentrations of the medium, which is the key to achieving the metastable fluid-fluid crtical point where the crystal nucleation begins. Simulation studies based on the physical mechanism reveals the formation of crystal nucleus by using the same approach[105] based on Bennett-Chandler scheme to compute the rate of activation process.

Wolde and Frenkel[105] through simulation studies using proteins as model system found that the rate limiting step in crystal nucleation is crossing the free energy barrier, and the formation of metastable fluid-fluid critical point represents the point of lowest free energy barrier to generate the critical crystal nucleus as shown in the Figure 3-14**:** .

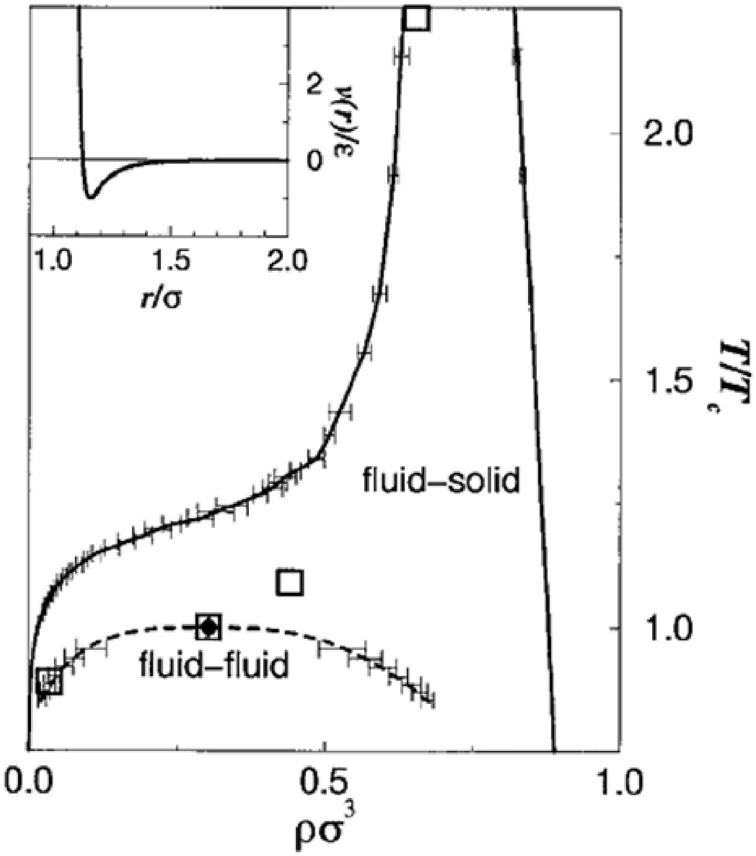

Figure 3-14: Phase diagram with short-range attraction. The diamonds indicate the fluid-fluid critical points. The solid lines indicate the equilibrium coexistence curves. The dashed curve indicates the metastable fluid-fluid coexistence (adapted from[105])

The cubic crystal formation in our system using peptides and gold nanoparticles depends on the solvent conditions. This narrow range of pH and ionic strength modulates the range of interaction, where the formation of meta-stable fluid- fluid critical point takes place.

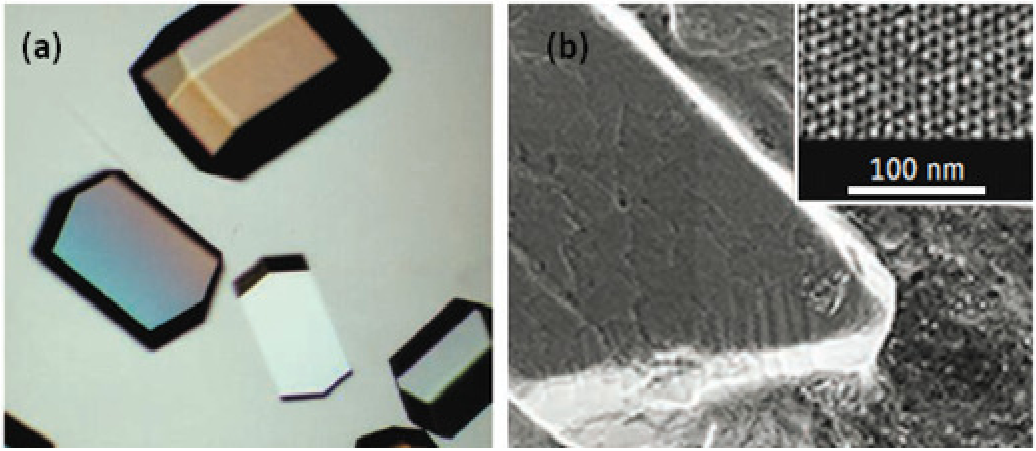

Figure 3-15: (a) Protein crystals of lysozyme obtained under slightly attractive interactions, and (b) a nanoparticle crystal assembled under controlled electrostatic attraction (adapted from[122]).

3.5 Conclusion

In conclusion, the reason why the range of experimental conditions to generate cubes from peptides and Au NPs is very narrow because the range of effective interactions mediating the crystal formation highly depends on the pH and salt concentrations of the medium which in our case falls in this narrow range.

3.6 Experimental Conditions

The triple helix was suspended in phosphate-buffered saline buffer with a concentration of 2.5mg/ml.Five different pH conditions of 3, 5.5, 7, 8.5 and 13.2 was monitored by adjusting the pH with phosphoric acid (pH 3), phosphate (pH 7), tris buffered saline (pH 8.5) NaOH (pH 13.2).The gold nanoparticle was purchased from Nanocs Inc with a concentration of 0.5 mg/ml. The conjugated nanoparticle solution was diluted to 1:10 with 0.1mM HEPES (pH 7).Incubation of the triple helix with the peptide was carried out for 1 hr at 4°C. A drop of the Au NP-peptide sample (4 µl) was applied to a carbon coated formvar copper TEM grid (Electron Microscopy Sciences, PA) and dried with filter paper and examined by TEM and electron diffraction (JOEL 1200 EX) at 100KV. For high resolution TEM imaging, an acceleration voltage of 200 KV was applied with a JOEL JEM-2100 LaB6 TEM.

CHAPTER 4: The Effect of NP Size on Protein-NP Assembly

4.1 Introduction

The complex material assembly using protein as the building block has a wide range of applications in fields of bio- based sensors [123], diagnostics, and biomarkers.[124.125] The availability of a wide range of sizes of nanoparticles and the ease of use of multiple ligands that can be specifically linked on the surface of nanoparticles provides the ability to tune the optical, magnetic, and electric properties of the biomaterial by controlling the nanoparticle spacing[126], structure, and function[127] of the device.

We are interested in examining the effect of the NP size on the peptide–Au NP assembly by using streptavidin-bound gold nanoparticles (Au NPs) of a diameter of 30 nm instead of 10 nm with the same ratio as previously described of 1:2 nanoparticle to peptide. The main goal of this experiment is to change the shape of the unit cell and the structure of resulting NP superlattices by introducing larger NPs. It is plausible that the larger size of Au NPs changes the peptide-peptide and peptide-NP interactions as well as the angle to bind the peptide at N-terminus, resulting in re-configuration of peptide-NP unit cells from bcc to some other forms.

4.2 Result and Discussion

4.2.1 Transmission Electron Microscopy (TEM)

When streptavidin-bound gold nanoparticles in a diameter of 30 nm were incubated with the biotinylated triple-helix peptide, whose length is 40 nm, in solution for one hour in a ratio of 1:2, they assembled into a well defined micron-sized hexagonal structure (Figure 4-1).

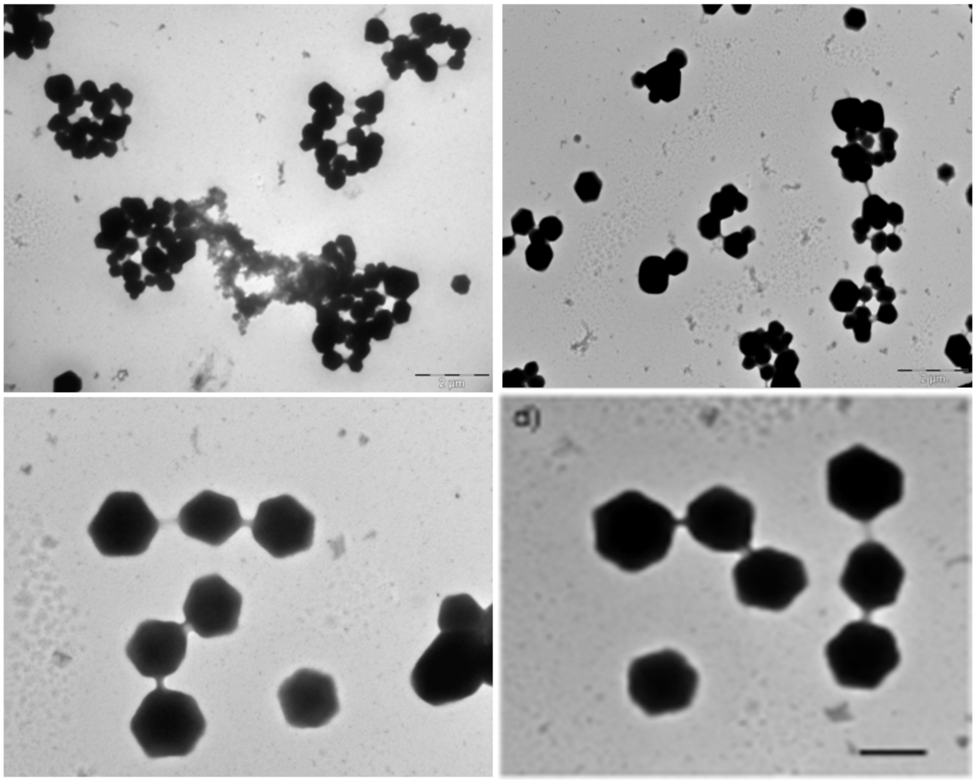

Figure 4-1: TEM images of the hexagons assembled from the biotinylated triple-helix peptides and the 30nm streptavidin-functionalized Au NPs.

4.2.2 Monitoring the peptide-NP assembly process in solution by Ultraviolet-Visible Spectroscopy (UV-Vis)

To study the dynamic nature of assembly of functionalized gold nanoparticles and the peptide, we monitored the SPR bands of Au NPs with time by collecting UV/Vis absorption spectra every 10 min on the sample with the relative concentration of 1:2 nanoparticles to peptide. Figure 4-2 reveals that a red shift starts to appear around 45 minutes.

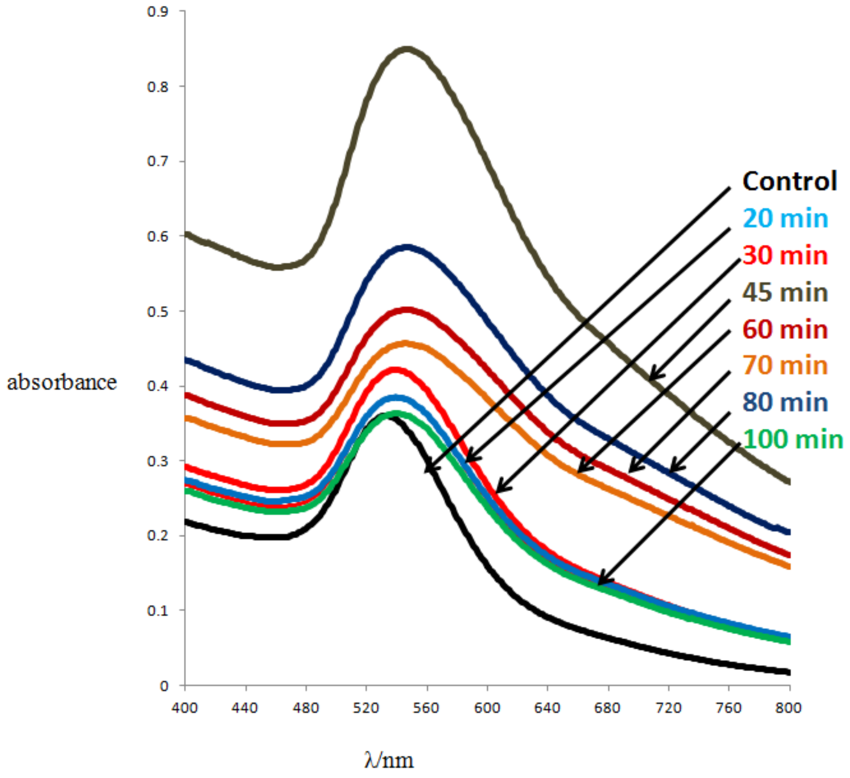

Figure 4-2: UV-Vis absorption spectra of the BAP877 and streptavidin-bound gold nanoparticles at different time at pH 7.4. Control shows the characteristic absorbance of neat gold nanoparticle at 528nm.

When the same assembly was carried out using F877 which does not possess the N-terminal Biotin Acceptor Peptide to interact with streptavidin on the gold nanoparticles, the UV-Vis did not show any apparent red shift Figure 4-3. These control experiments indicate that the red shift in Figure 4-2 is due to assembly of the biotinylated peptides and streptavidin coated Au NPs.

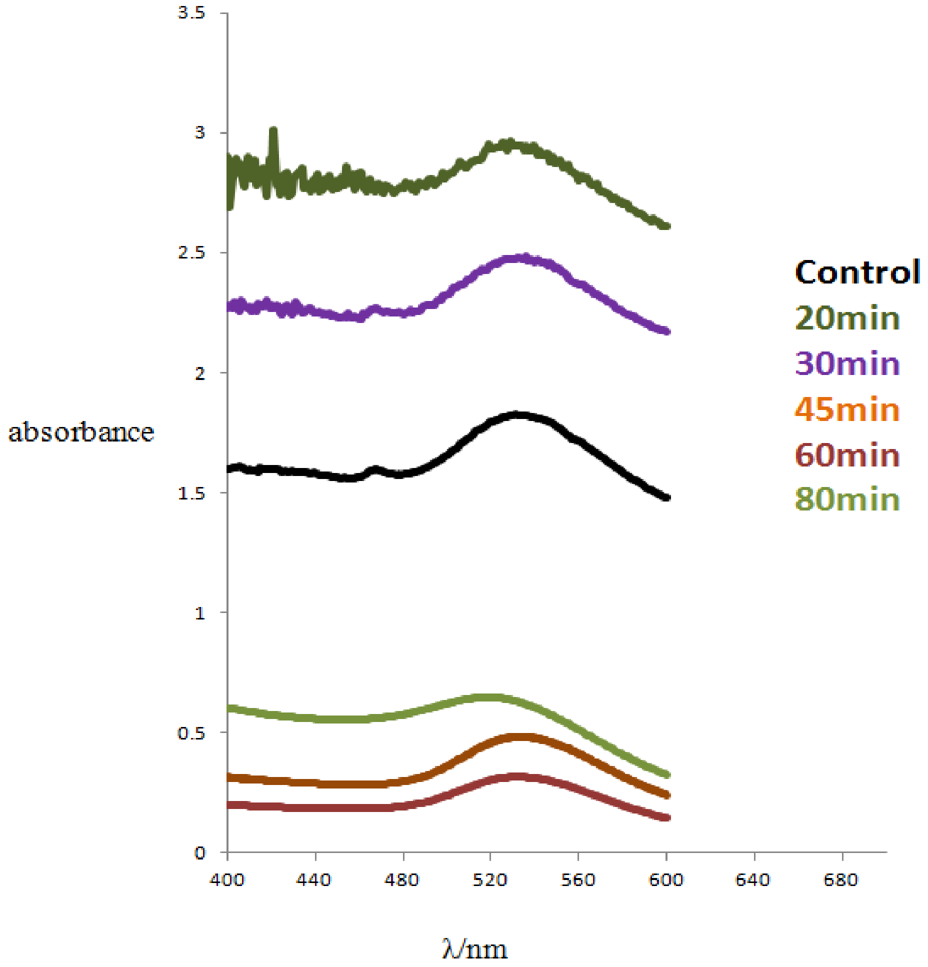

Figure 4-3: UV-Vis absorption spectra of the F877 (no biotin) and streptavidin-bound gold nanoparticles at different time at pH 7.4. Control shows the characteristic absorbance of gold nanoparticle at 528nm.

4.2.3 The peptide-NP assembly at various time with TEM studies

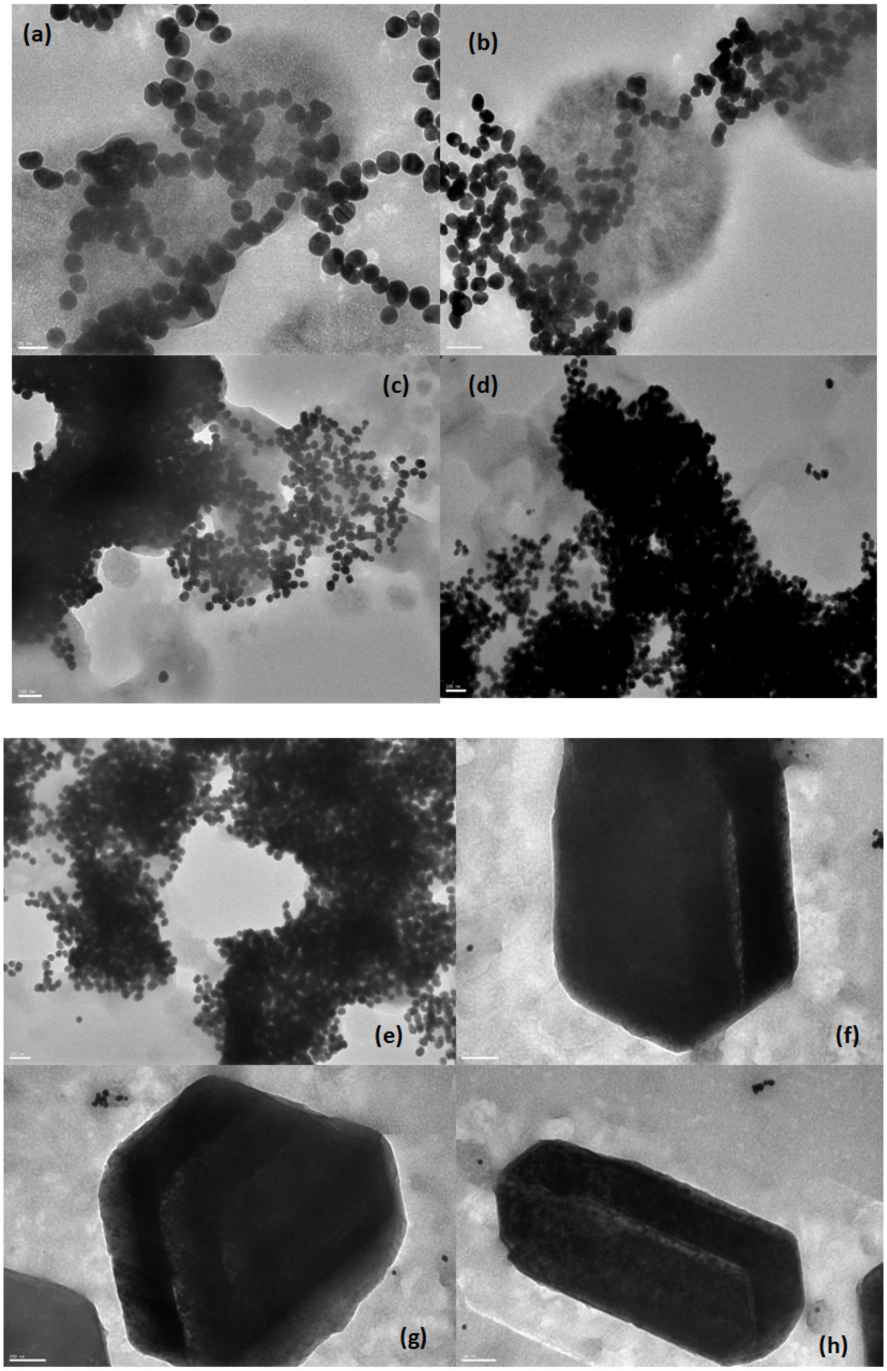

Figure 4-4: TEM images of the assembly of biotinylated triple-helix peptides with streptavidin-functionalized gold nanoparticles at various time (a) 20 minutes, (b) 30 minutes, (c) & (d) 45minutes, (scale bar 100nm) (e), (f), and (g) 60 minutes, and (h) 80 minutes (scale bar 200nm) at pH 7.4.

Figure 4-4 shows the TEM micrographs of assembly of biotinylated triple helix with streptavidin bound gold nanoparticles at various time intervals at pH 7.4.These TEM micrographs reveal that at 45 minutes the assembly is leading to the formation of mainly 3D architectures as shown in Figure 4-4 and also the red shift observed with time as seen from the UV-vis absorption spectra. Figure 4-2

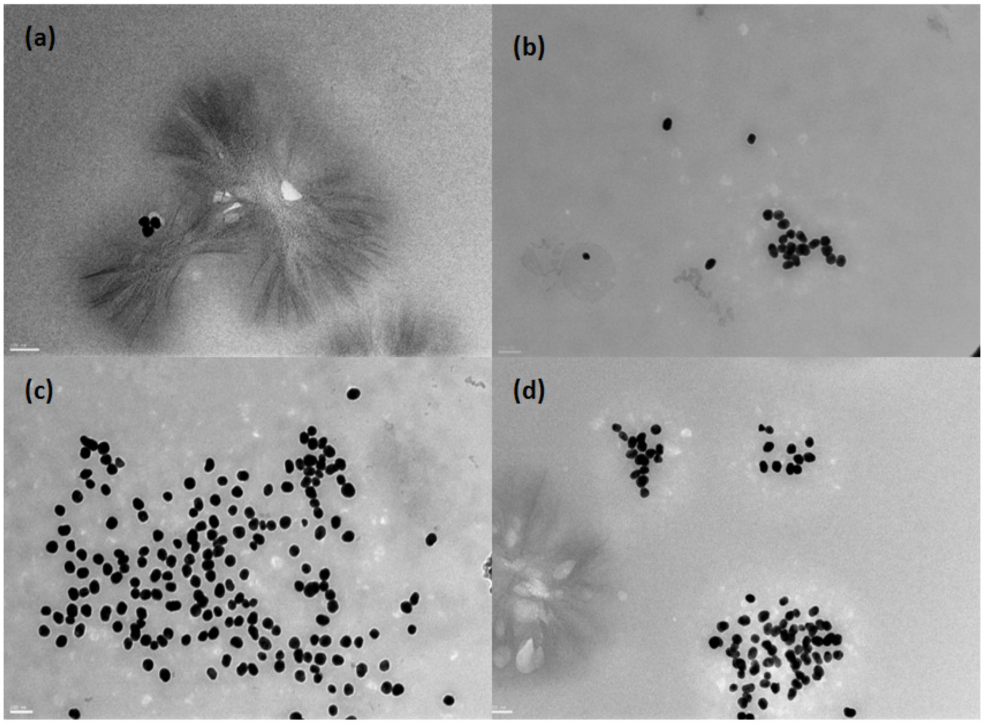

Figure 4-5: TEM images of control experiments with non-biotinylated triple-helix peptide (F877) with streptavidin-functionalized gold nanoparticles at various time (a) 20 minutes, (b) 30 minutes, (c) 60 minutes, and (d) 80 minutes (scale bar 100nm).

Figure 4-5 shows the TEM micrographs of F877 triple helix which does not have the N-terminus Biotin Acceptor Peptide and therefore cannot bind to streptavidin on gold nanoparticles.[128] When the assembly was carried out at pH 7.4 with the same ratio of 1:2 of nanoparticles to peptide as performed for the BAP877-Au NP experiments, we did not observe any red shift as seen from the UV-vis absorption spectra from 20 to 80 minutes (Figure 4-3). Also the time dependent TEM studies (Figure 4-5), did not result in any characteristic assembly because of the absence of biotin acceptor peptide at the N-terminus of the peptide. Therefore, it cannot interact with the streptavidin bound gold nanoparticles.

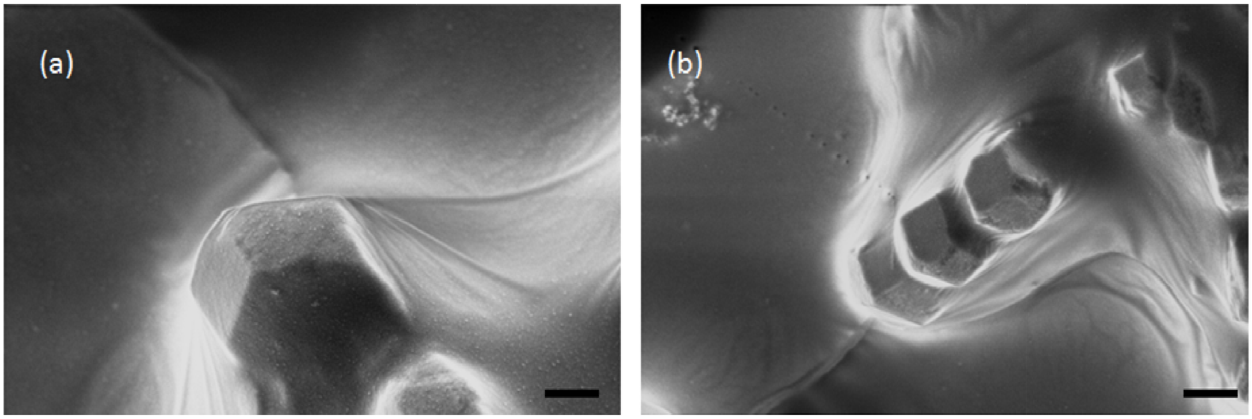

Figure 4-6: SEM images of the hexagonal structure of the peptide Au NP assembly.

SEM images in Figure 4-6 shows that the peptides and Au NPs are assembled into the 3D hexagonal prism as consistent with the TEM observation. Since the final structure is the hexagonal prism, it is highly likely that Au NPs are assembled into Hexagonal Closed Packing (HCP).

4.3 Hexagonal Closed Packing (HCP) Unit Cell of Au NPs and peptides

The hexagonal close packed structure is a close packed structure by piling layers in the A - B - A - B - A - B . . . . . sequence. To build 3-dimensional structures, the close packed layers need to be stacked on the top of the bottom layer to have the spheres in one layer fit into the tetrahedral holes of the layer as shown in Figure 4-7.

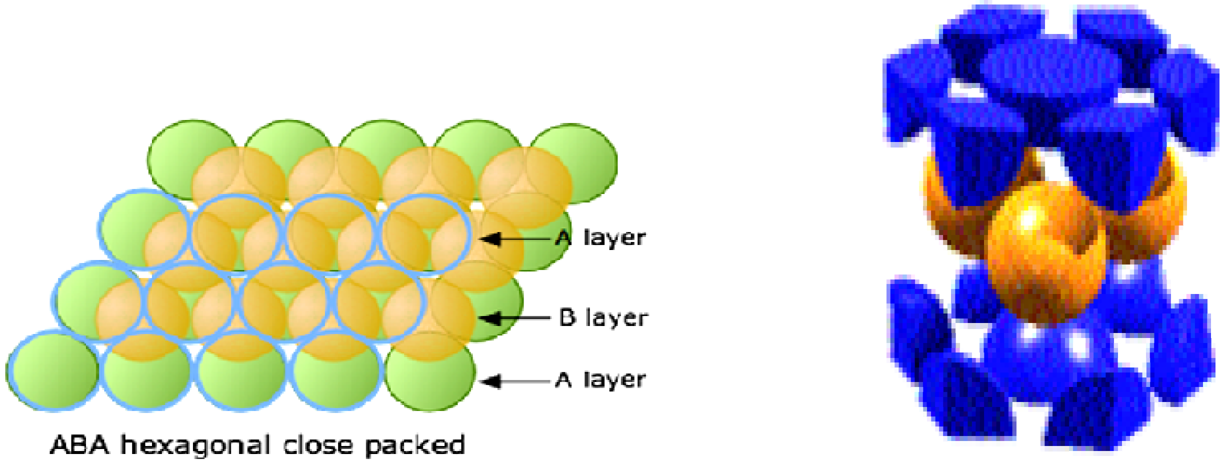

Figure 4-7: HCP unit cell with the A - B - A - B layer stacking.

After piling the first layer "A" and the second layer ("B"), the third layer can be added to fit into the holes of the B layer such that the atoms lie above those in layer A. By repeating this arrangement one obtains the A - B - A - B - A - B stacking or hexagonal close packing. Each HCP unit cell is comprised of 6 spheres.

4.3.1 Octahedral and Tetrahedral Holes

An HCP unit cell has two types of holes:-a) Octahedral holes and b) Tetrahedral Holes as shown in the Figure 4-8. There are 6 octahedral holes and 12 tetrahedral holes per HCP unit cell.

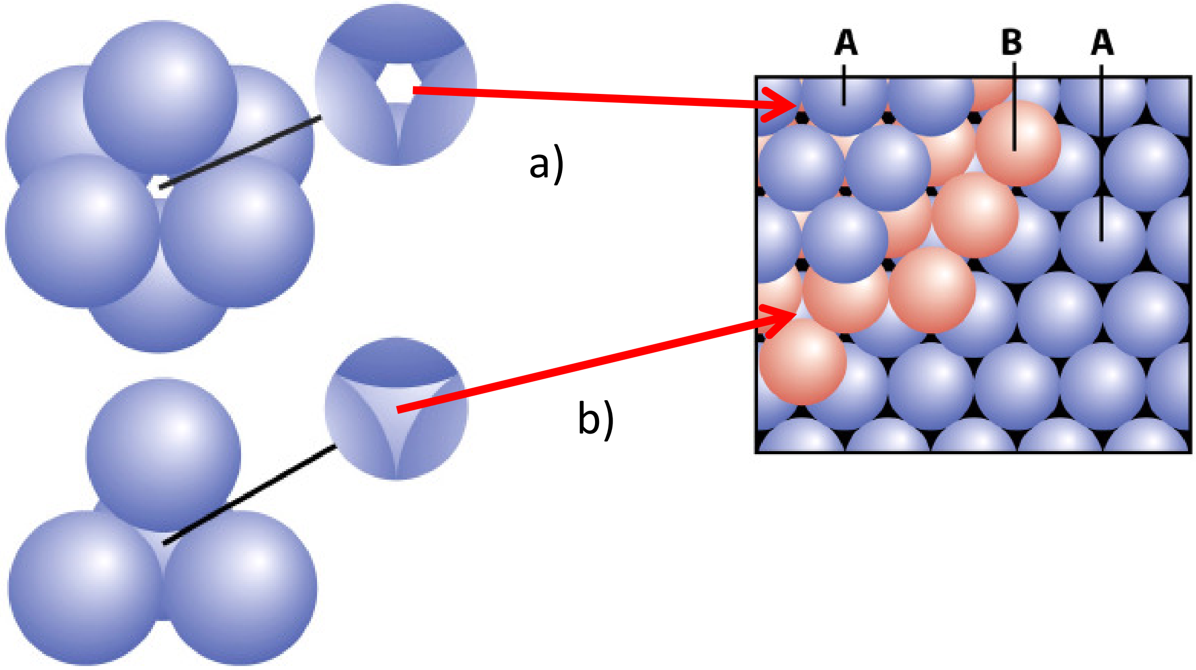

Figure 4-8: a) Octahedral holes in HCP; b) Tetrahedral holes in HCP

4.3.2 Calculation of Space of Octahedral Hole between Au NPs to Accommodate Peptides

4.3.2.1 Derivation

Let us derive the relationship between the radius (r) of the octahedral void and the radius (R) of the gold nanoparticle with streptavidin in hexagonal close packing (HCP).

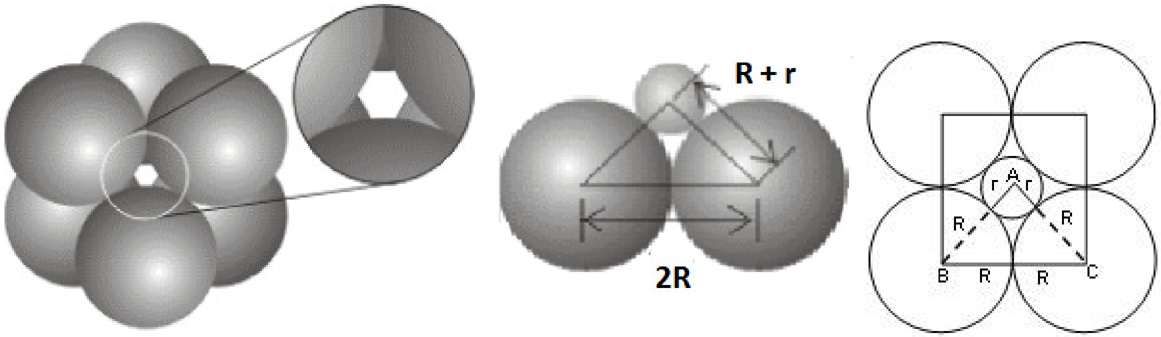

Figure 4-9: Octahedral holes – Width Calculation

A sphere of radius (r) of the octahedral void is shown in the Figure 4-9.

By applying Pythagoras theorem the radius can be derived as:-

$BC^2 = AB^2 + AC^2$

$\Rightarrow (2R)^2 = (R + r)^2 + (R + r)^2$

$\Rightarrow (2R)^2 = 2(R + r)^2$

$=> \sqrt{2}R = R + r$

$=> r = \sqrt{2}R - R = (1.414 - 1) R$

$r = 0.414 R$

Where, r is the radius of the octahedral void and R is the radius of the Gold nanoparticle with streptavidin

When the diameter of the nanoparticle is 30 nm and streptavidin around the nanoparticles is ~5nm, the combined diameter of the nanoparticles and streptavidin is approximately 40 nm. Therefore using the above derived formula ($r = 0.414 R$), the diameter of an octahedral hole is calculated as 16.56nm**.**

4.3.3 Calculation of Width of Tetrahedral Hole

4.3.3.1 Derivation

Let us derive the relationship between the radius (r) of the tetrahedral void and the radius (R) of the gold nanoparticle with streptavidin in hexagonal close packing (HCP).

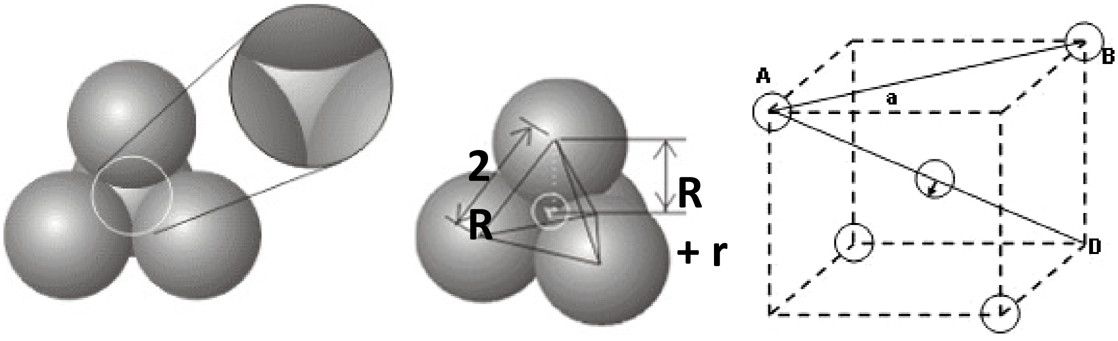

Figure 4-10: tetrahedral holes – Width Calculation

When a sphere of radius (r) exist in the tetrahedral void and a tetrahedral void is represented in a cube as shown in the Figure 4-10, the fourth lies on the top and the sphere occupies the tetrahedral void.

Let the length of the side of the cube = a

From right angled triangle ABC, face diagonal

$$AB = \sqrt{(AC^2 + BC^2)} = \sqrt{(a^2 + a^2)} = \sqrt{2}a$$

As spheres A and B are touching each other, face diagonal $AB = 2R$

$\Rightarrow 2R = \sqrt{2}a$ or $R = a/\sqrt{2}$ .... (i)

Again from the right angled triangle ABD

$AD = \sqrt{(AB^2 + BD^2)} = \sqrt{((\sqrt{2}a)^2 + a^2)} = \sqrt{3}a$

But as small sphere (void) touches other spheres, evidently body diagonal $AD = 2(R + r)$. This implies $2(R + r) = \sqrt{3}a$

Hence, $R + r = \sqrt{3}/2\ a$ ... (ii)

Dividing equation (ii) by equation (i)

$R + r/R = \sqrt{3} / 2 \times a / a / \sqrt{2} = \sqrt{3} / \sqrt{2}$

$\Rightarrow 1 + r/R = \sqrt{3} / \sqrt{2} = 1.225 \Rightarrow r/R = 1.225 - 1 = 0.225$

$\Rightarrow r = 0.225\ R$

Where r is the radius of the tetrahedral void and R is the radius of the gold nanoparticle with streptavidin

When the diameter of the nanoparticle is 30 nm and streptavidin around the nanoparticles is ~5nm, the combined diameter of the nanoparticles and streptavidin is approximately 40 nm. Therefore using the above derived formula ($r = 0.225 R$), the diameter of a tetrahedral hole would be 9 nm.

4.3.4 Calculation of Height of HCP Unit cell

4.3.4.1 Derivation of the Height of an octahedral hole

Let us derive the relationship between the height (c) of HCP unit cell and the radius (R) of the gold nanoparticle with streptavidin in hexagonal close packing (HCP).

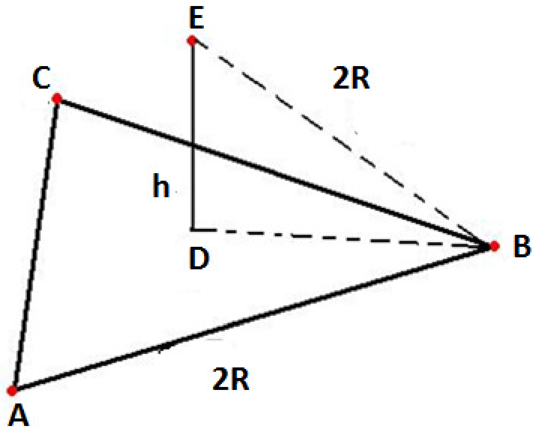

Figure 4-11: Height Calculation for HCP unit cell

A, B, C, E represents the centers of sphere of atoms in HCP closed packing,

Now, AB=BC=CA=EB = 2R (edge lengths of HCP)

BD=2R/√3, as BD divides the median through B in 2:1 ratio from B. Now, EDB is right angle triangle, so by Pythagoras theorem:

$$(2R/\sqrt{3})^2 + h^2 = (2R)^2$$

$h= 2R\sqrt{2/3}$

Now, there will be another atom which will be mirror image of E on plane ABC, Therefore, the height (c) of HCP will be 2h

$c =2h = 4R \sqrt{2/3}$

Where, R is the radius of the Gold nanoparticle with streptavidin

Since the diameter of the nanoparticle is 30 nm and streptavidin around the nanoparticles is ~5nm, the diameter of the nanoparticles combined with streptavidin will now be approximately 40 nm. Therefore using the above derived formula, the height of the HCP unit cell is 65.2 nm.

Because the hcp has repeating layers of the AB-AB pattern, the depth of the hole depends on the number of superlattice layers. As the third layer is A again and sits exactly on the top of the first A layer, this geometry does not completely cover the octahedron hole and therefore the peptide can be assembled with Au NPs by occupying this space .

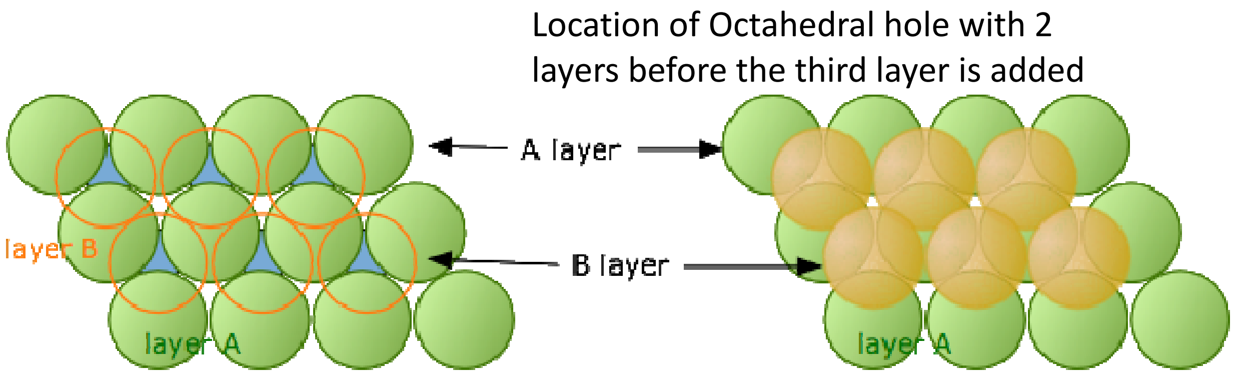

Figure 4-12: Octahedral holes in HCP

In this conformation, as the octahedral holes penetrate on the AB-AB layer, the height of octahedral hole per unit cell would be around 65.2nm, which has enough space to accommodate the peptide**.**

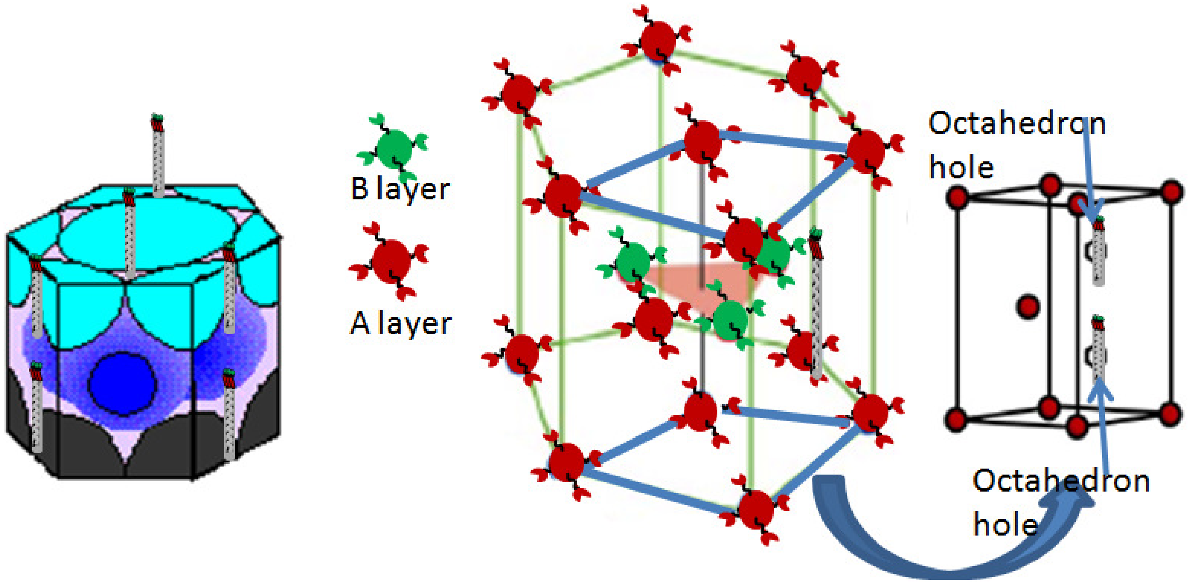

Figure 4-13: Illustration of peptides and streptavidin-bound gold nanoparticles in a hexagonal closed packed structure.

4.4 Simulation Studies

The red-shift in the normalized absorption peaks with time shown in Figure 4-2 represents the inter-particle spacing change which is approximately 543 nm. Edward Furlani group (University of Buffalo) computed the absorption peak positions as a function of the interparticle distance using a finite-element based electromagnetic modeling. From this result, the inter particle space in the hcp NP assembly is estimated (Table 4-1)

HCP Spacing Parameter ‘s’	Absorption Peak	Shift
5 nm	553 nm	25 nm
7.5 nm	543 nm	15 nm
10 nm	540 nm	10 nm

Table 4-1: Absorption peak positions as a function of inter-particle distance using finite-element based electromagnetic modeling.

Unassembled 30 nm Au nanoparticle shows a peak at 528 nm. When the wavelength of the red shift is computed as 15 nm, the inter-particle spacing is 7.5 nm. This shift agrees best with our space calculation results for surface to surface inter particle distance range of 6.75 nm to 9 nm for a tetrahedral hole. Therefore, we conclude on the basis of the simulation that the Au NPs are packed in the hcp structure with the spacing of 7.5 nm.

References

---

[1]J. H. Chen and N. C. Seeman (1991). Nature. 350: 631.

[2] S. Y. Park (2008). Nature 451: 553.

[3]D. Nykypanchuk, M. M. Maye, et al. (2008). Nature 451: 549.

[4] H. Matsui, S. Pan, et al. (2000). Journal of Physical Chemistry B 104: 9576.

[5] E. Gazit (2002). Current Medicinal Chemistry 9: 1667.

[6] E. Gazit (2002). Angew. Chem. Int. Ed. 41: 257.

[7] W. Shenton, S.A. Davis, et al. (1999). Advanced Materials 11(6): 449.

[8] J. Yang, M. Mayer, et al. (2004). Angew. Chem. Int. Ed. 43(12): 1555.

[9] S. Hegde, S. Kapoor, et al. (2006). Journal of Colloid and Interface Science 297(2): 637.

[10] Y. Wang, Z. Y. Tang, et al. (2005). Nano Letters 5(2): 243.

[11] S. Mark, M. Bergkvist, et al. (2006). Biomacromolecules 7(6): 1884.

[12] D. B. Allred, M. Sarikaya, et al. (2005). Nano Letters 5(4): 609.

[13] M. Platt, G. Muthukrishnan, et al. (2005). Journal of the American Chemical Society 127(45): 15686

[14] S.Behrens, W. Habicht, et al. (2006). Advanced Materials 18(3): 284

[15] Connolly and D. Fitzmaurice (1999). Advanced Materials 11(14): 1202.

[16] J. Park, A. A. Lazarides, et al. (2001). Angew. Chem. Int. Ed. 40(15): 2909.

[17] Smorodin, U. Beierlein, et al. (2005). Nanotechnology 16(8): 1123.

[18] Salem, A. K,Chen, M,Hayden, et al. (2004). Nano Letters 4 (6):1163.

---

[19] K. T. Nam, B. R. Peelle, et al. (2004). Nano Letters 4(1): 23.

[20] P. J. Yoo, K. T.Nam, et al. (2006). Nature Materials 5(3): 234.

[21] C. M. Niemeyer (2001). Angew. Chem. Int. Ed. 40: 4128

[22] P. R. Wolde and D. Frenkel (1997). Science: 277.

[23] M. G. Sandros, D. Gao , et al. (2005). Journal of the American Chemical Society 127: 12198

[24] M. Zayats, E. Katz, et al. (2005). Journal of the American Chemical Society 127: 12400

[25] . Dyadyusha, H. Yin, et al. (2005). Chemical Communications: 3201.

[26] K. R. Lytton-Jean and C. A. Mirkin (2005). Journal of the American Chemical Society 127: 12754.

[27] C. J. Ackerson, M. T. Sykes, et al. (2005). Proc. Natl. Acad. Sci. USA 102: 1338391C. J. Ackerson, M. T. Sykes, et al. (2005). Proc. Natl. Acad. Sci. USA 102: 13383

[28] C. M. Niemeyer (2001). Angew. Chem. Int. Ed. 40: 4128.

[29] M. Sastry, M. Rao, et al. (2002). Acc. Chem. Res. 35: 847.

[30] E. Katz and I. Willner (2004). Angew. Chem. Int. Ed. 43: 6042.

[31] T. Pellegrino, S. Kudera, et al. (2005). Small 1: 48.

[32] A. Verma and V. M. Rotello (2005). Chemical Communications: 303

[33] C. You, M. De, et al. (2005). Current Opinion in Chemical Biology 9: 639.

[34] N. L. Rosi and C. A. Mirkin (2005). Chem. Rev. 105: 1547.

---

[35] P.W. Barone, S. Baik, et al. (2005). Nature Materials 4: 86.

[36] K. Besteman, J.O. Lee, et al. (2003). Nano Letters 3: 727

[37] F. Patolsky and C. M. Lieber (2005). Mater Today 8: 20.

[38] E. Gazit (2007). Imperial College Press, London.

[39] A. M. Kalsin, M. Fialkowski, et al. (2006). Science **312**: 420.

[40] J. Aizenberg, J. C. Weaver, et al. (2005). Science **309**: 275.

[41] J. J. De Yoreo and P. M. Dove (2004). Science **306**: 1301.

[42] F. C. Meldrum and H. Colfen (2008). Chem. Rev. **108**: 4332.

[43] M. B. Dickerson, K. H. Sandhage, et al. (2008). Chem. Rev. **108**: 4935.

[44] R. A. Miller, A. D. Presley, et al. (2007). Journal of the American Chemical Society **129**: 3104.

[45] F. A. Aldaye, A. L. Palmer, et al. (2008). Science **321**: 1795.

[46] E. S. Andersen, M. Dong, et al. (2009). Nature **459**: 73.

[47] J. Sharma, R. Chhabra, et al. (2009). Science **323**: 112.

[48] W. M. Shih, J. D. Quispe, et al. (2004). Nature **427**: 618.

[49] R. P. Goodman, M. Heilemann, et al. (2008). Nature Nanotechnology **3**: 93.

[50] Y. He, T. Ye, et al. (2008). Nature **452**: 198.

[51] I. Severcan, C. Geary, et al. (2009). Nano Letters **9**: 1270.

[52] D. Nykypanchuk, M. M. Maye, et al. (2008). Nature **451**: 549.

---

[53] A. J. Mastroianni, S. A. Claridge, et al. (2009). Journal of the American Chemical Society **131**: 8455.

[54] J. Zheng, J. J. Birktoft, et al. (2009). Nature **461**: 74.

[55] S. Y. Park, A. K. R. Lytton-Jean, et al. (2008). Nature **451**: 553.

[56] C. Lin, Y. Liu, et al. (2009). Biochemistry **48**: 1663.

[57] X. Gao and H. Matsui (2005). Advanced Materials **17**: 2037.

[58] A. V. Persikov and B. Brodsky (2002). Proc. Natl. Acad. Sci. USA **99**: 1101.

[59] D. E. Birk and P. Bruckner (2005). Top. Curr. Chem. **247**: 185.

[60] A. Goldberg, J. Salerno, et al. (1989). Gene **80**: 30.

[61] M. T. Krejchi, E. D. T. Atkins, et al. (1994). Science **265**: 1427.

[62] A. Panitch , K. Matsuki, et al. (1997). Macromolecules **30**: 42.

[63] M.J. Buehler (2006). Proceedings of the National Academy of Sciences USA. **103**: 12285.

[64] H. Bai, K. Xu, et al. (2007). Angew. Chem. Int. Ed. **119**: 3383.

[65] K. Xu, I. Nowak, et al. (2008). J. Biol. Chem. **283**: 34337.

[66] D. Beckett, E. Kovaleva, et al. (1999). Protein Sci. **8**: 921.

[67] Y. Maeda, T. Yoshino, et al. (2008). Appl. Environ. Microbiol. **74**: 5139.

[68] P. J. Schatz (1993). Nature Biotechnology **11**: 1138.

[69] D. Beckett, E. Kovaleva, et al. (1999). Protein Sci. **8**: 921.

---

[70] Y. Maeda, T. Yoshino, et al. (2008). Appl. Environ. Microbiol. **74**: 5139.

[71] B. A. Grzybowski, C. E. Wilmer, et al. (2009). Soft Matter **5**: 1110.

[72] C. D. Keating, K. M. Kovaleski, et al. (1998). J. Phys. Chem. B **102**: 9404.

[73] S. Chan, M. R. Hammond, et al. (2005). N. Chem. Biol. **12**: 323.

[74] M.Q. Zhu, L.Q. Wang, et al. (2004). Journal of the American Chemical Society 126: 2656.

[75] R.R. Bhattacharjee, M. Chakraborty, et al. (2006). J Phys. Chem. B 110: 6768.

[76] N. Nath and A. Chilkoti (2001). Journal of the American Chemical Society 123: 8197.

[77] J. Simard, C. Briggs, et al. (2000). Chem. Commun.: 1943.

[78] H. Hiramatsu and F. E. Osterloh (2003). Langmuir **19**: 7003

[79] G. Li, T. Wang, et al. (2003). Colloid Polym. Sci. **281**: 1099.

[80] S. Mandal, A. Gole, et al. (2001). Langmuir **17**: 6262.

[81] C.R. Mayer, S. Neveu, et al. (2004). Colloid Interface Sci. **273**: 350.

[82] J. Kijowski (1993). Int. J. Food Sci.Technol. **28** 587.

[83] J. F.V. Vincent (1982). McMillan Press Ltd.London **38**.

[84] Manju Grover Venugopal and John A. M. Ramshaw (1994). Biochemistry **33**(25): 7949.

[85] E. Y. Jones and A. J. Miller. (1991). J. Mol. Biol. **218**: 209.

[86] M. G. Venugopal, J. A. M. Ramshaw, et al. (1994). Biochemistry **33**: 7948.

[87] A. V. Persikov, J. A. M. Ramshaw, et al. (2005). Biochemistry **44**: 1414.

[88] E. P. Katz and C. W. David. (1990). Biopolymers **29**: 791.

[89] E. Bianchi and G. Conio. (1967). J. Biol. Chem. **242**: 1361.

---

[90] C. A. Miles, T. V. Burjanadze, et al. (1995). J. Mol. Biol. **245**: 437.

[91] E. I. Tiktopulo and A. V. Kajava. (1998). Biochemistry **37**: 8147.

[92] K. J. Lumb and P. S. Kim (1995). Science **268**: 436.

[93] C. D. Waldburger and J. F Schildbach (1996). Nat. Struct. Biol. **2**: 122.

[94] P. F. Davison (1989). Connect Tissue Res. **18**: 293.

[95] R. Usha and T. Ramasami (2000). Journal of Applied Polymer Science **75**: 1577.

[96] K. Xu, I. Nowak, et al. (2008). Journal of Biological Chemistry **283**: 34337.

[97] H. R. Elden (1971). Wiley: New York.

[98] E.D. Aberle and E.W. Mills (1983). Recip. Meat Conf. Proc. **36** 125.

[99] R.L. Willett (2005). Proc. Natl. Acad. Sci. U. S. A. **102**: 7817.

[100] X. Fu, Y. Wang, et al. (2003). Angew. Chem. Int. Ed. **15**: 902.

[101] G. N. Ramachandran, B. B. Doyle, et al. (1968). Biopolymers **6**: 1771.

[102] E J. Engel, H. T. Chen, et al. (1977). Biopolymers **16**: 601.

[103] E. Leikina, M. V. Mertts, et al. (2002). Proc. Natl. Acad. Sci. U. S. A. **99**(3).

[104] S. Frank, R. A. Kammerer, et al. (2001). J. Mol. Biol. **308**: 1081.

[105] Pieter Rein ten Wolde and D. Frenkel (1997). SCIENCE **277 1975**.

[106] K. Ogasahara, E.A. Lapshina et al. (1998). Biochemistry **37**(17): 5939.

[107] T. Miller, E. Karmas, et al. (1983). J. Food Sci. **48** 681.

[108] P.B. Kenney, R.L. Henrickson, et al. (1986). J. Food Sci. **15** 277.

[109] A. Finch and D.A. Ledward (1973). Biochim. Biophys. Acta **295** 296.

[110] E. V. Shevchenko, D. V. Talapin, et al. (2006). Nature **439**: 55.

[111] A. George and W. Wilson (1994). Acta Crystallogr. D **50**: 361.

[112] A.A. Chernov and H. Komatsu (1995). Science and Technology of Crystal Growth: 329.

---

[113] N. M. Green (1990). Methods Enzymol **184**: 51.

[114] Uwe Freudenberg, Sven H. Behrens, et al. (2007). Biophysical Journal **92** 2108.

[115] N. Aktas (2003). Thermochimica Acta. **407**: 105.

[116] S. Kumar and R. Nussinov. (2002). ChemBioChem. **3**: 604.

[117] Prerna Kaur, Yoshiaki Maeda, et al. (2010). Angew. Chem. Int. Ed. **49**: 8375.

[118] S. Leikin, D.C. Rau, et al. (1995). Nature Struct. Biol. **2**: 205.

[119] E. V. Shevchenko, D. V. Talapin, et al. (2006). Nature **439**: 55.

[120] A. George and W. Wilson (1994). Acta Crystallogr. D. **50**: 361

[121] Franz Rosenberger (1996). Journal of Crystal Growth **166**: 40.

[122] Orlin.D.Velev (2006). Science **312**: 376.

[123] C. J. Murphy, A. M. Gole, et al. (2008). Acc. Chem. Res. **41**: 1721.

[124] R. A. McMillan, C. D. Paavola, et al. (2002). Nat. Mater. **1**: 247.

[125] M. H. Hu, L. P. Qian, et al. (2007). Angew. Chem. Int. Ed. **46**: 5111.

[126] A.Verma, S.Srivastava, et al. (2005). Chem. Mater. **17**: 6317.

[127] S. Srivastava, B. Samanta, et al. (2007). J. Am. Chem. Soc. **129**: 11776.

[128] Kihyun Kwon, Kang Yeol Lee, et al. (2007). J. Phys. Chem. C **111**: 1161.